Diesel passenger vehicle shares influenced COVID-19 changes in urban nitrogen dioxide pollution

Gaige Hunter Kerr[1*], Daniel L. Goldberg[1], K. Emma Knowland[2,3], Christoph A. Keller[2,3], Dolly Oladini[4], Iyad Kheirbek[5], Lucy Mahoney[4], Zifeng Lu[6], Susan C. Anenberg[1]

[1] Department of Environmental and Occupational Health, Milken Institute School of Public Health, The George Washington University, Washington, DC, USA
[2] Universities Space Research Association (USRA)/GESTAR, Columbia, MD, USA
[3] NASA Goddard Space Flight Center (GSFC), Global Modeling and Assimilation Office (GMAO), Greenbelt, MD, USA.
[4] C40 Cities, London, England, UK
[5] C40 Cities Climate Leadership Group Inc., New York, NY, USA
[6] Systems Assessment Center, Energy Systems Division, Argonne National Laboratory, Lemont, IL, USA

[*] Author to whom correspondence should be addressed

Abstract: Diesel-powered vehicles emit several times more nitrogen oxides than comparable gasoline-powered vehicles, leading to ambient nitrogen dioxide (NO_2) pollution and adverse health impacts. The COVID-19 pandemic and ensuing changes in emissions provide a natural experiment to test whether NO_2 reductions have been starker in Europe, a region with larger diesel passenger vehicle shares. Here we use a semi-empirical approach that combines *in-situ* NO_2 observations from urban areas and an atmospheric composition model within a machine learning algorithm to estimate business-as-usual NO_2 during the first wave of the COVID-19 pandemic in 2020. These estimates account for the moderating influences of meteorology, chemistry, and traffic. Comparing the observed NO_2 concentrations against business-as-usual estimates indicates that diesel passenger vehicle shares played a major role in the magnitude of NO_2 reductions. European cities with the five largest shares of diesel passenger vehicles experienced NO_2 reductions ~2.5 times larger than cities with the five smallest diesel shares. Extending our methods to a cohort of non-European cities from the C40 Cities network reveals that NO_2 reductions in these cities were generally smaller than reductions in European cities, which was expected given their small diesel shares. We identify potential factors such as the deterioration of engine controls associated with older diesel vehicles to explain spread in the relationship between cities' shares of diesel vehicles and changes in NO_2 during the pandemic. Our results provide a glimpse of potential NO_2 reductions that could accompany future deliberate efforts to phase out or remove passenger vehicles from cities.

Graphical abstract:

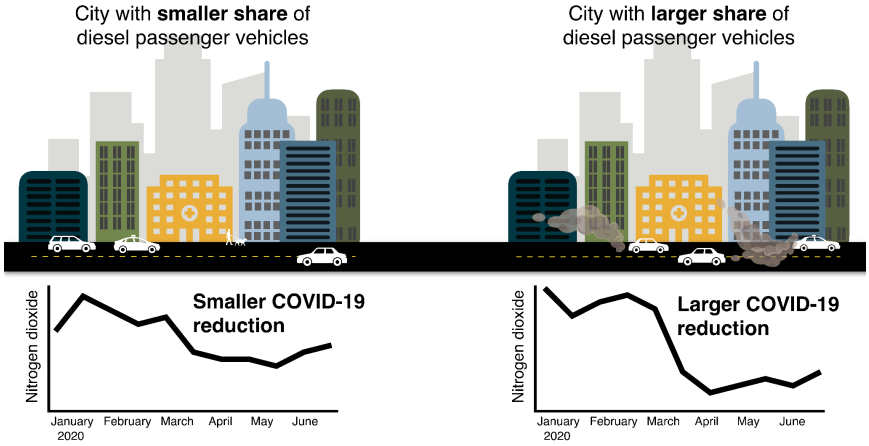

Keywords: Urban air quality, machine learning, environmental modeling, atmospheric chemistry, nitrogen dioxide, COVID-19, diesel

Section 1 Introduction

Ambient nitrogen dioxide (NO_2) pollution is a global concern for public health, particularly in urban areas, and is linked with decreased lung function, cardiopulmonary and respiratory disease, and pediatric asthma, among other adverse health effects (Faustini et al., 2014; Achakulwisut et al., 2019; Khomenko et al., 2021). Traffic emissions are often the dominant source of urban NO_2, followed by emissions from industrial sources and energy production and usage (Degraeuwe et al., 2019). As such, NO_2 is an effective surrogate for the broad traffic-related mix of pollutants.

Changes in urban NO_2 during the pandemic (hereafter "ΔNO_2") varied greatly across the world (e.g., Ding et al., 2020; Keller et al., 2021a; Kerr et al., 2021; Vadrevu et al., 2021). Direct comparisons of ΔNO_2 among cities are inherently complicated by the meteorological patterns (Goldberg et al., 2020), stay-at-home measures, and culture unique to each city. However, even after accounting or normalizing for these important moderating factors, differences in ΔNO_2 likely remain. With all else equal, one cause of these differences is vehicle fuel type. Reductions in NO_2 have purportedly been larger in regions dominated by diesel vehicles (Kroll et al., 2020).

Diesel-powered passenger vehicles emit substantially greater emissions of nitrogen oxides ($NO_x \equiv NO + NO_2$) than comparable gasoline-powered vehicles (Weiss et al., 2011). For example, real-world measurements indicate that Euro 6 diesel vehicles emit ten times more NO_x than Euro 6 gasoline vehicles (European Environment Agency, 2016). Since the late 1990s, European nations experienced a "diesel boom" followed by a recent decline. The share of diesel-powered passenger vehicles (henceforth "diesel shares") steadily increased until the Volkswagen emissions scandal was brought to light in 2015. Since then, diesel shares of new car registrations have declined in Europe (Jonson et al., 2017; Tietge and Díaz, 2017). Diesel NO_x, including emissions in excess of certification limits, has contributed to high NO_2 pollution in Europe (e.g., Kiesewetter et al., 2014; Carslaw et al., 2016; Degraeuwe et al., 2017; von Schneidemesser et al., 2017) and adverse health impacts (e.g., Anenberg et al., 2017; Jonson et al., 2017). In several countries outside of Europe such as the United States, Canada, and China, diesel shares are much

smaller, and gasoline (petrol) is the primary fuel consumed by passenger vehicles (e.g., McDonald et al., 2014).

In this study, we examine how the COVID-19 pandemic can reveal the fingerprint of diesel passenger vehicles on NO_2 pollution in urban areas. The pandemic, which largely affected the transportation sector due to stay-at-home measures, provides an unprecedented natural experiment that allows us to tease out the relationship between urban vehicle fleets and ΔNO_2. Additionally, we highlight future data and research needs to better enable global-scale studies on clean transportation and air quality.

Section 2 Materials and Methods

Section 2.1 Materials

We select 22 focus cities spanning 17 European countries (Table S1, Figure S1) based on the availability of (1) *in-situ* NO_2 observations, (2) country-level diesel shares, and (3) city- or country-level traffic trends during the pandemic. We then combine city-specific data with meteorological fields and surface pollutant concentrations from the NASA GEOS Composition Forecast Modeling System (GEOS-CF; Keller et al., 2021b) to estimate the relationship between diesel shares and ΔNO_2 across all focus cities (Figure 1).

We generally choose one city per country (usually the capital or largest city) as publicly available databases on diesel shares at the subnational level do not exist or are difficult to obtain. However, for some countries (e.g., Germany, Italy) we select two cities within a county if both cities have their own traffic trends to illustrate how different meteorology and changes in traffic impact results.

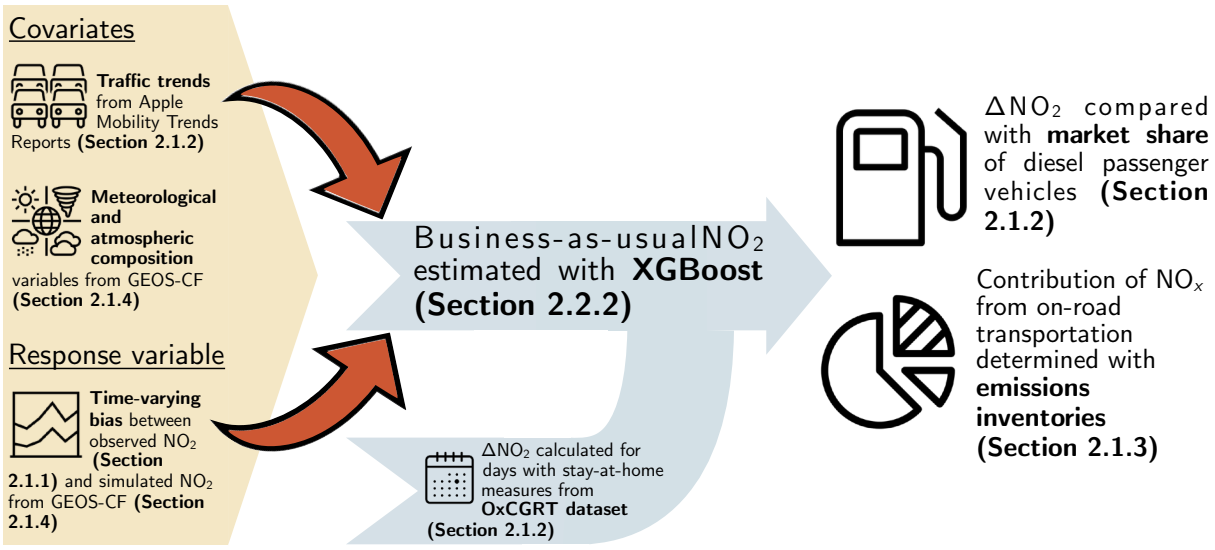

Figure 1. Process diagram showing the materials and methods used to quantify influence of diesel passenger vehicle shares on changes in NO_2 during COVID-19.

Section 2.1.1 NO_2 observations

We obtain observed hourly NO_2 concentrations from 1 January 2019 to 30 June 2020 from the European Environment Agency (European Environment Agency, 2018). The number of NO_2 monitors in each city considered for this study varies from 2 (Zagreb, Croatia) to 126 (London, United Kingdom) with an average of ~13 monitors per city (Table S1, Figure S1). To the best of our knowledge, all monitors are regulatory-grade (not low-cost). The designation of a monitor as belonging to a particular city is determined using municipality or equivalent unit definitions from the Nomenclature of Territorial Units for Statistics, a hierarchical system for delineating administrative units in Europe. While we primarily feature this European cohort of cities in our study due to the need to have a range in diesel shares, we complement this cohort with four additional cities in the Americas and Oceania that are part of the C40 Cities network (SI Text).

Section 2.1.2 Diesel, traffic, and stay-at-home data

We rely on national-level diesel shares for the most recent year available (generally 2019) from the European Automobile Manufacturers Association and International Council on Clean Transportation (Diaz et al., 2020; European Automobile Manufacturers Association, 2021). Our focus on passenger vehicle diesel shares stems from the fact that (1) most *heavy-duty vehicles*, regardless of country, use diesel fuel (European Automobile Manufacturers Association, 2021) whereas there is a wide range of *passenger vehicles* diesel shares (Table S1), and (2) one of the most salient impacts of the pandemic was on the passenger vehicle sector given the shift to remote work for many jobs (e.g., Liu et al., 2020; Kerr et al., 2021). Using national-level data assumes that diesel shares are homogeneous throughout individual countries and does not account for regional or local policies (e.g., low emission zones in city centers) that may target diesel vehicles. If more than one city from a particular country is used in our study, these cities have the same diesel shares.

We account for changes in traffic emissions on NO_2 concentrations using Apple COVID-19 Mobility Trends Reports (Apple, 2020), which provide daily traffic trends relative to a baseline volume from 13 January 2020 (Figure S2). We select the highest level of available granularity for a given city. Of our 22 focus cities, 19 have traffic data aggregated to the city-level, and we use national-level data for the other three cities (Table S1). This dataset has been previously used to examine the impacts of different degrees of social distancing on COVID-19 spread (Cot et al., 2021) and air quality (Venter et al., 2020).

The timing of stay-at-home measures and lockdowns varies across and within countries, and we use the Oxford COVID-19 Government Response Tracker (OxCGRT) to provide country-specific dates of stay-at-home recommendations and requirements (Hale et al., 2021). OxCGRT discretizes stay-at-home measures into four categories ranging from “no measures” to “required to not leave the house with minimal exceptions” (Figure S2). When calculating ΔNO_2 in a particular focus city, we average over all dates where stay-at-home measures are either recommended or required through 30 June 2020 and refer to this period as “lockdown.”

Section 2.1.3 Emissions inventories

We use three gridded emissions inventories to understand how NO_x emissions from light-duty passenger vehicles contribute to total anthropogenic NO_x emissions in each city using NO_x

emissions from on-road transportation as a proxy for light-duty passenger vehicle emissions. These three inventories are the Emission Database for Global Atmospheric Research v5.0 (EDGAR; Crippa et al., 2019, 2020), the Community Emissions Data System 2020 v1 (CEDS; Hoesly et al., 2018, McDuffie et al., 2020), and the European Monitoring and Evaluation Programme (EMEP; Mareckova et al., 2017).

These inventories vary in their resolution, extent, and available time period. We use CEDS (0.5˚ × 0.5˚ globally) and EMEP (0.1˚ × 0.1˚ across Europe) annual mean emissions from 2017 and EDGAR (0.1˚ × 0.1˚ globally) for 2015 (latest year available). The inventories use spatial and temporal surrogates such as population density and road networks to spatially-allocate country-level emission estimates to grid cells. Given uncertainties associated with these surrogates (e.g., Geng et al., 2017) we degrade EDGAR and EMEP to 0.5˚ × 0.5˚ and present results using both regridded and native resolutions to explore how these spatial proxies affect the estimated importance of on-road transportation to total NO_x emissions.

Specifically, we first sample the inventories' estimates of NO_x from on-road transportation and total anthropogenic NO_x emissions at grid cells colocated with NO_2 monitors within an individual city. Then, we sum each of these two components over the grid cells containing monitors within a city and thereafter form a city-averaged ratio representing the contribution from on-road transportation to total NO_x within that city. While these three inventories use some common data inputs, including all indicates how different methods and assumptions may impact the estimated contribution of on-road transportation to total NO_x emissions.

Section 2.1.4 GEOS-CF

NASA's GEOS-CF v1.0 provides three-dimensional gridded historical estimates of meteorology and atmospheric composition at 0.25˚ x 0.25˚ (~25 km) horizontal resolution globally from the surface to about 80 km for the period since 1 January 2018 (Keller et al., 2021b). This is possible because the GEOS-Chem chemical transport model (Bey et al., 2001) is fully integrated into the GEOS Earth System Model (Keller et al., 2014; Long et al., 2015; Hu et al., 2018). We obtain near-surface (lowest model level) hourly-average meteorological and atmospheric composition fields (Table S2) from GEOS-CF from 1 January 2019 to 30 June 2020 and thereafter sample the model for the grid-box closest to the location of each air quality monitor within individual cities shown in Figure S1.

It is important to note that the meteorology and fire emissions are constrained by observations; in particular, the inclusion of fire radiative power based on MODIS from the Quick Fire Emissions Dataset (QFED; Darmenov and da Silva, 2015) informs the model of recent fires. Anthropogenic NO_x emissions are generally derived from the global Hemispheric Transport of Air Pollution inventory (HTAP; Janssens-Maenhout et al., 2015). HTAP v2.2 harmonizes the complete global coverage of EDGAR with the latest-available regional inventories. GEOS-CF v1.0 incorporates the monthly HTAP v2.2 anthropogenic emissions from 2010 for all subsequent years and applies weekly and diurnal scaling factors (Keller et al., 2021b). Therefore, the model has no knowledge about COVID-19 restrictions impacting anthropogenic emissions but does have realistic meteorology and fire emissions for 2019 and 2020 and thus represents a business-as-usual scenario for the COVID-19 period (see also Keller et al., 2021a). Full details regarding the

GEOS-CF configuration and available model output are described by Keller et al. (2021a,b) and Knowland et al. (2020), respectively.

Section 2.2 Methods

To investigate the influence of diesel shares on ΔNO_2 we must form a counterfactual that represents business-as-usual NO_2 and accounts for differences in local meteorology, atmospheric composition, and traffic between 2019 and 2020, as these factors influence NO_2 concentrations independently of fuel type (Gkatzelis et al., 2021). Our methods, described below, detail how we leverage our semi-empirical data within a machine learning framework to account for the important factors influencing NO_2 (Figure 1).

Section 2.2.1 Data Postprocessing

We average observed NO_2 and modeled meteorology- and composition-related variables to daily mean values from hourly time slices beginning 0000 UTC. For each focus city, all variables taken from *in-situ* monitors or model grid cells colocated with monitors are spatially averaged to produce a "meta-site" following Ivatt and Evans (2020) that represents daily observed or modeled NO_2, meteorology, and composition at the city level.

Our machine learning technique trains on data from 2019; however, the Apple mobility dataset begins on 13 January 2020. To remedy this issue, we calculate mean day-of-the-week-specific traffic volumes from 13 January 2020 to 29 February 2020 to capture volumes prior to most stay-at-home measures (e.g., Figure S2) and thereafter apply these day-of-the-week-specific volumes to 1 January 2019 - 12 January 2020. While this reconstructed time series is imperfect and may miss seasonal variations or holidays, it captures weekday-weekend patterns, which are important for urban NO_2.

Section 2.2.2 Machine Learning Algorithm

Following Ivatt and Evans (2020) and Keller et al. (2021a), we employ eXtreme Gradient Boosting (XGBoost; Chen and Guestrin, 2016) to predict the time-varying GEOS-CF NO_2 bias against observations in 2019 as a function of the input variables in Table S2. We thereafter estimate business-as-usual NO_2 in 2020 that accounts for meteorological-, chemical-, and traffic-driven variability.

Specifically, for each city meta-site, we use a *k*-fold cross validation technique to predict the time-varying bias between GEOS-CF and observed NO_2 with the following steps:

1) Data from 1 January to 31 December 2019 are decomposed into six 2-month folds. We split the data into consecutive folds, without reshuffling, to avoid overfitting due to the autocorrelation present in the data. The first fold is reserved for validation, and we build a bias-corrected model using the remaining five folds as a training dataset. Previous work has demonstrated that one year of data is adequate for bias-correcting an atmospheric composition model to observations (Ivatt and Evans, 2020).
2) We quantify model performance using a variety of metrics with the reserved (testing) fold and training folds (Figure S3).

3) We use the bias-corrected model derived from each fold to predict the bias for the entire measuring period (1 January 2019 - 30 June 2020).
4) The first three steps are repeated five times (thus, every fold of the dataset is treated as a test), resulting in a total of six bias-corrected models. We average bias-corrected NO_2 concentrations over these six folds (Keller et al., 2021a,b).

As GEOS-CF represents a business-as-usual scenario (Section 2.1.4), once we have bias-corrected modeled NO_2, we can understand what observed NO_2 concentrations in 2020 *should* have been without COVID-19 (Keller et al., 2021a). We thereafter calculate ΔNO_2 as

$$(NO_{2,\,observed} - NO_{2,\,business\text{-}as\text{-}usual})/NO_{2,\,business\text{-}as\text{-}usual} \times 100\%. \quad \text{(Equation 1)}$$

We perform this calculation every day during country-specific recommended or required stay-at-home measures and average over this subset of days.

Since XGBoost is unable to extrapolate beyond the training range (Ivatt and Evans, 2020), it is most appropriate to consider ΔNO_2 as accounting for weekday-weekend variations in traffic but not for the plummeting traffic volumes in spring 2020. To determine whether traffic volumes from Apple Mobility Trends Reports serve as a proxy for the day of the week, we also perform a sensitivity analysis in which we recalculate ΔNO_2 using the day of the week (e.g., Monday = 0, Tuesday = 1, etc.) as an input variable rather than traffic volumes.

We exploit SHapley Additive exPlanations (SHAP) values to increase the interpretability of business-as-usual NO_2 concentrations. SHAP values employ game theory to explain the contribution of individual input variables in predicting the bias (Shapely, 1953; Lundberg and Lee, 2016; Lundberg and Lee, 2017). For each of the *k* folds in each city and for each day, SHAP values are assigned to each input variable used to generate the predicted bias between GEOS-CF and observed NO_2 representing the marginal contribution of each input variable. Variables with larger absolute SHAP values therefore have a greater influence on correcting the bias between GEOS-CF and observed NO_2.

Section 3 Results

GEOS-CF captures daily NO_2 variability in our focus cities (Figure S4), reinforcing its ability to aid in understanding lockdown-related NO_2 changes. We highlight London to further illustrate GEOS-CF's capabilities and our methods (Figure 2a). The temporal correlation (*r*) between modeled and observed NO_2 in 2019 for London is 0.78 ($r = 0.60$ averaged over all cities; Figure S3b). Despite the good correlation, there is a low model bias relative to observations in many of our focus cities (mean fractional bias = -0.60 averaged over all cities; Figure S3a). GEOS-CF's low bias is well-documented, especially in Europe and North America where there are publicly available observations (Keller et al., 2021b). This bias may stem from model resolution; uncertainties in atmospheric transport, boundary layer height, vertical mixing, emissions, and chemistry; and monitor interference with other nitrogen-containing compounds (Dunlea et al., 2007; Lamsal et al., 2008; Keller et al., 2021a).

Using XGBoost to correct the bias in simulated NO_2 and generate bias-corrected concentrations leads to substantially better agreement against observations than the native GEOS-CF concentrations, and the aforementioned low model bias is greatly reduced. Figure 2a illustrates the excellent agreement between business-as-usual and observed NO_2 in 2019 prior to the

lockdown. The mean fractional bias for London in 2019 is reduced from -0.41 with the native GEOS-CF concentrations to -0.02 with the bias-corrected concentrations, and we note similar improvements in other focus cities (Figures S3-S4).

We characterize the relative contribution of input variables in generating the business-as-usual NO_2 concentrations by SHAP values (Figure 2b). The ranking of input variables by their median SHAP values indicates local atmospheric transport and species related to basic ozone (O_3) chemistry (e.g., O_3, NO_2, carbon monoxide) are the most important variables for inferring business-as-usual NO_2 concentrations for both London and all focus cities (Figure 2b).

Traffic emerges as one of the top influencing variables in estimating business-as-usual concentrations (Figure 2b). The relative contribution of traffic in London ranks lower than for the aggregation of SHAP values over all focus cities, but the distribution has right-skew with a wide range for large SHAP values (Figure 2b). This result indicates that intraweek variations in traffic are one of the most important variables in correcting the bias and producing business-as-usual NO_2 concentrations for certain days in our measuring period and particular folds of the *k*-fold cross validation.

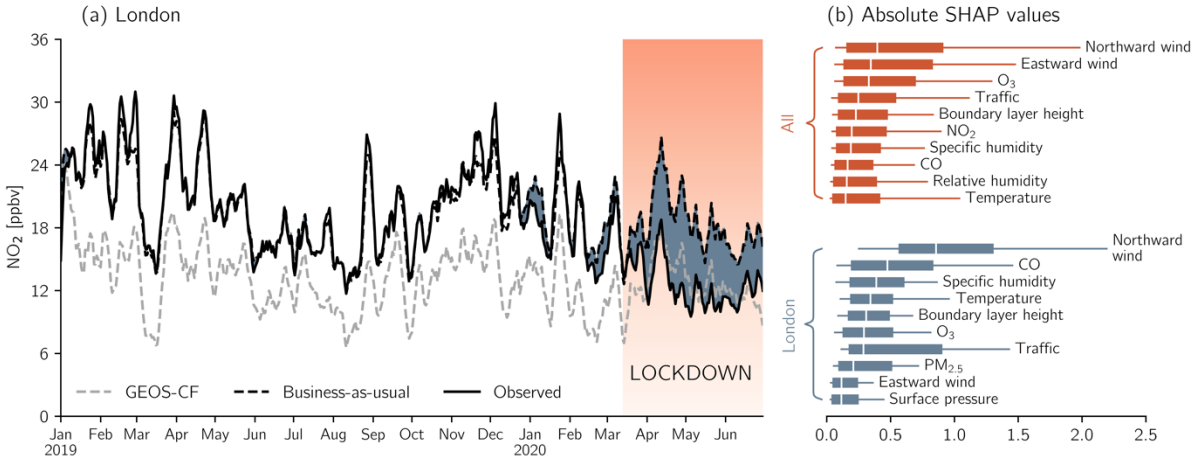

Figure 2. Illustration of XGBoost-inferred business-as-usual concentrations and drivers of these predictions. *(a) Observed, GEOS-CF, and business-as-usual NO_2 concentrations in London. Time series represent the daily average of all in-situ monitors or their colocated model grid cells in London. The shaded red band denotes the 2020 lockdowns in the United Kingdom, and blue shading corresponds to days where observed NO_2 is less than business-as-usual NO_2 to highlight the COVID-19 lockdowns. (b) SHAP value distributions for the ten most important meteorology-, composition-, and traffic-related XGBoost input variables for all focus cities (top) and London (bottom) are ranked by their median value, here indicated by vertical white lines. Boxes show the interquartile range, and whiskers extend to the 10th and 90th percentiles.*

Observed NO_2 concentrations begin to diverge from business-as-usual concentrations in London around mid-February 2020, slightly preceding the United Kingdom's declaration of recommended stay-at-home measures (compare Figures 2a, S2). When averaged over the lockdowns, ΔNO_2 between the observed and business-as-usual concentrations is -28.5% in London. Observed NO_2 concentrations exhibit departures from business-as-usual concentrations in spring 2020 in other cities as well but with varying magnitudes (Figure S4).

Our focus cities span a spectrum of pre-lockdown NO_2 pollution levels and diesel shares ranging from 8.1% in Athens, Greece to 69.2% in Vilnius, Lithuania (Figure 3, Table S1). Mean 2019 NO_2 in all 22 focus cities exceeded the recently-revised World Health Organization annual mean NO_2 guideline value of 10 $\mu g\ m^{-3}$ ($\approx$ 5.3 ppbv, assuming an ambient temperature of 298.15 K and pressure of 1013.25 hPa). Even Helsinki, which has the lowest 2019 NO_2 concentration ($\approx$ 8.4 ppbv) of all focus cities, exceeds this guideline value on the order of 60%.

The average pandemic-related NO_2 reductions (ΔNO_2) across cities is -23.8% (standard deviation = 16.0%), and the precise magnitude ranges by approximately 60% across cities. We next compare ΔNO_2 with cities' diesel shares and see a clear pattern emerge: cities with larger diesel shares tend to have larger ΔNO_2, while ΔNO_2 is smaller in cities with smaller diesel shares (r = -0.50, p = 0.02; Figure 3). For example, the average reduction in NO_2 ($\overline{\Delta NO_2}$) in cities with the top five largest diesel shares ($\overline{\Delta NO_2}$ = -38.1%) is ~2.5 times larger than the reduction in cities with the five smallest shares ($\overline{\Delta NO_2}$ = -15.0%). The slope of the linear regression fit between ΔNO_2 and diesel shares provides a succinct summary of our results (Figure 3). This slope indicates that the lockdowns led to ΔNO_2 of approximately -5.3% for every 10% increase in diesel shares (Figure 3).

A drawback of the linear regression lies in its intercept, which suggests a very small change in NO_2 for cities whose shares of diesel passenger vehicles are close to 0%. Even cities with these small shares, such as those in North America with mostly gasoline-powered passenger vehicles, experienced substantial decreases in NO_2. For example, Goldberg et al. (2020) found a median NO_2 decrease of ~22% in major North American cities during spring 2020 after adjusting for seasonality and meteorology. In all cities, other sources of urban NO_x beyond diesel passenger vehicles (e.g., heavy-duty vehicles, power plants, maritime activity, industry) not accounted for in our experimental design contributed to ΔNO_2, regardless of the diesel passenger vehicle share.

Vilnius, Lithuania is among the most notable outliers in Figure 3, potentially due to a large heating plant upwind of Vilnius' *in-situ* NO_2 monitors (Figure S1), which burns natural gas and mazut, a highly polluting, low quality fuel oil. Berlin, Germany also stands out given the small ΔNO_2 during the pandemic (ΔNO_2 = -2.9%). This result could stem from the varied siting of Berlin's *in-situ* monitors (Figure S1), which were all included in our city meta-site (Section 2.2.1). In a recent study, NO_2 reductions during the pandemic were not significant at urban background monitors in Berlin despite large significant decreases at monitors near traffic (von Schneidemesser et al. 2021).

We next describe sensitivity analyses that speak to the robustness of our results. Testing whether traffic volumes from Apple Mobility Trends Reports can capture weekday-weekend differences in traffic patterns affirms the ability of this dataset to serve as a proxy for the day of the week and XGBoost to capture these intraweek variations (Figure S5). The OxCGRT lockdown dates represent country-level dates for stay-at-home measures if at least some region of a given country has the restrictions (Hale et al., 2021). Responsibility for COVID-related restrictions was often delegated to state or local governments; however, to the best of our knowledge, no globally consistent database with city-specific lockdown dates exists. Given uncertainties associated with these dates, we simply recalculate ΔNO_2 for a uniform time period extending from 15 March

2020 to 15 June 2020 and find substantively similar results (compare Figures 3, S6). We examine the extent to which ΔNO_2 varied between *recommended* versus *required* stay-at-home measures shown in Figure S2 and the impacts of restriction type on the diesel share-ΔNO_2 relationship. Again, we observe no substantive changes (compare Figures 3, S7).

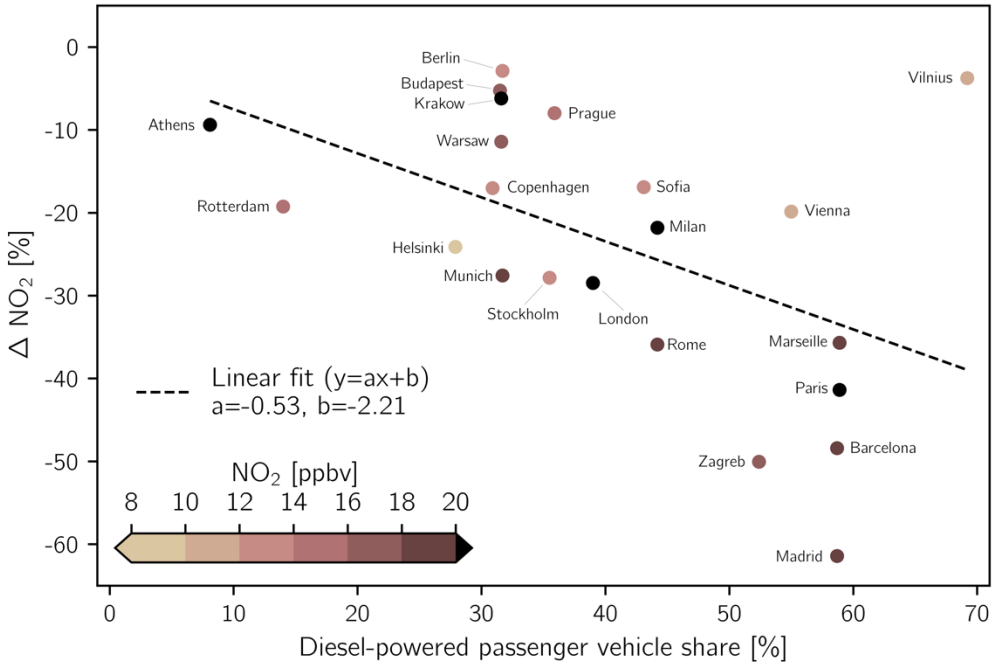

Figure 3. Association of passenger vehicle diesel share with changes in NO_2 (ΔNO_2) during the pandemic. *Points are colored by annual mean NO_2 concentrations in 2019. Inset text indicates the form and coefficients of the linear regression used to describe the relationship between diesel shares and ΔNO_2.*

We test whether including the cohort of select C40 Cities (Mexico City, Los Angeles, Auckland, and Santiago; see SI Text) is consistent with the relationship between diesel shares with ΔNO_2 we found in European cities. These additional cities specifically allow us to test whether our findings are generalizable to cities with different cultural and behavioral practices (e.g., reliance on public transit, adherence to COVID-19 containment measures) and lower diesel shares compared to the European cohort focused on elsewhere in this study.

Given the small diesel shares in these cities (cohort-averaged share = 4.0%; Table S1), we expect they would experience small to modest NO_2 reductions. This is indeed the case, and the cohort-averaged ΔNO_2 of -14.8% is markedly smaller than the reduction in many European cities with larger diesel shares (Figures S6-S7). This cohort of C40 Cities also demonstrates some of the challenges associated with inferring business-as-usual NO_2. For example, Los Angeles has one of the smallest diesel shares of all cities examined (Table S1) but experienced markedly larger NO_2 reductions than other cities with small diesel shares. We hypothesize that NO_x emissions related to the Ports of Los Angeles and Long Beach, the largest in North America and unaccounted for in our methodological framework, might inflate ΔNO_2 compared to cities

without ports or other large sources of NO_x. The topic of unconsidered moderating influences is explored in Section 4.

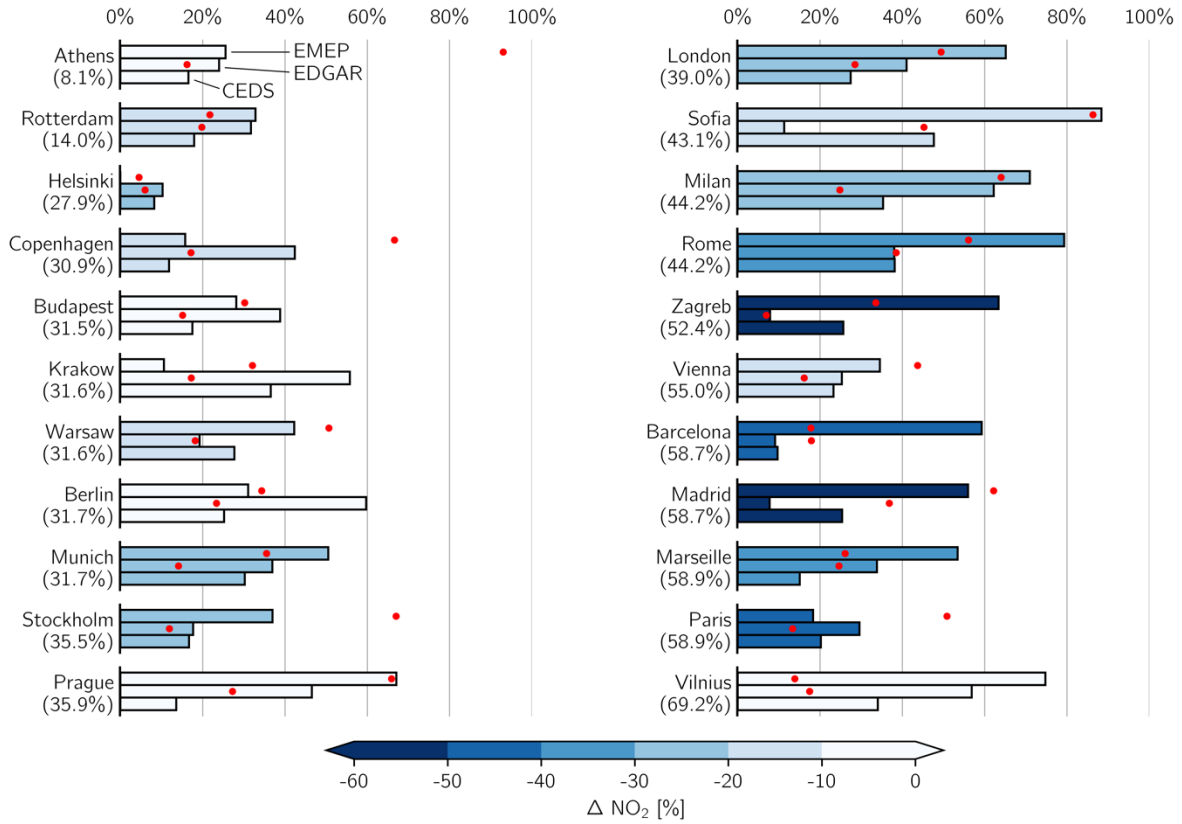

Figure 4. The contribution of on-road transportation to total NO_x emissions. *City-specific contributions are derived from three emissions inventories: 2017 EMEP regridded to 0.5˚ × 0.5˚ (top bar; see Athens for legend), 2015 EDGAR regridded to 0.5˚ × 0.5˚ (middle bar), and 2017 CEDS at its native resolution of 0.5˚ × 0.5˚ (bottom bar). Contributions estimated from EMEP and EDGAR at their native resolution of 0.1˚ × 0.1˚ are denoted as red points alongside the corresponding bars. Cities are ordered by their diesel passenger vehicle shares (also indicated below city names in parentheses) and colored by ΔNO_2 from Figure 3.*

We next explore a key factor that could explain the spread among cities' ΔNO_2 given their diesel shares. The contribution of on-road transportation to overall NO_x emissions varies across cities. On average, road transportation contributes 47% of total NO_x emissions in European cities but ranges from approximately 20% to 70% depending on the city (Degrauewe et al., 2019; Font et al., 2019). We hypothesize that two hypothetical cities with identical diesel shares, meteorology, and other moderating factors likely have different ΔNO_2 if the on-road transportation sector has a different-sized contribution to total NO_x emissions in these cities.

Testing whether the diesel shares-ΔNO_2 relationship together with the contribution of on-road transportation emissions to total NO_x emissions can explain the spread in our results yields inconclusive results (Figure 4). As an example, Madrid, Barcelona, Paris, and Marseille have similar diesel shares, but Madrid and Barcelona experienced larger ΔNO_2. Based on our

hypothesis, we expect that the contribution of on-road transportation would be larger in Madrid and Barcelona than in Paris and Marseille. This hypothesis indeed holds for these four cities holds when examining the EMEP inventory regridded to 0.5˚ × 0.5˚ but not for the other inventories or for all cities (Figure 4).

Degrading the EDGAR and EMEP inventories to a coarser resolution can also lead to stark differences in the estimated contribution of on-road transportation NO_x emissions, especially for cities near the land-sea interface. Copenhagen, Helsinki, and Stockholm are good examples of this behavior; the contribution suggested by EMEP at its native resolution is two or more times greater than the contribution suggested by EMEP regridded to 0.5˚ × 0.5˚ (Figure 4) due to the influence of the ocean, which has no NO_x emissions from on-road transportation.

Our analysis of these inventories also underscores the substantial spread among inventories' estimation of on-road transportation NO_x, even when regridding to regional (0.5˚ × 0.5˚) scales. EMEP often has the highest suggested contribution from on-road transportation of the three inventories (Figure 4). The suggested importance of on-road transportation can vary by a factor of five or more across inventories for the same city (e.g., compare EMEP and EGDAR estimates for Barcelona and Sofia). Discrepancies among inventories are well-documented (Elguindi et al., 2020), and differences could reflect the inventories' different time periods (2015 versus 2017) and uncertainties related to resolution, emission factors, or spatial proxies used to allocate emissions from regional totals to grid cells.

Section 4 Discussion

Our study demonstrates that diesel shares played a major role in the magnitude of ΔNO_2 experienced by cities during the COVID-19 natural experiment. The magnitude of bias-corrected ΔNO_2 varies from approximately -3% to -61% across cities, and ΔNO_2 is a factor of ~2.5 times larger in European focus cities with the top five diesel shares compared to cities in the bottom five. The relationship between diesel shares and COVID-related NO_2 reductions deduced from a sensitivity analysis that considers C40 member cities outside of Europe is in reasonable agreement with our results from Europe and suggests the generalizability of our findings. By leveraging this unique natural experiment, we are able to observe the relationship between NO_2 and diesel shares. This relationship gives an indication of the changes in NO_2 that could be expected if cities decrease their diesel shares through policy, economic forces (e.g., increased affordability of electric passenger vehicles), or social forces (e.g., diesel passenger vehicles viewed unfavorably as a result of "Dieselgate").

Major strengths of our analysis include our semi-empirical approach that leverages air quality data from monitoring networks as well as our use of a machine learning algorithm, XGBoost, to establish the relationship between NO_2 and local meteorology, atmospheric composition, and traffic trends. By combining XGBoost with GEOS-CF to infer business-as-usual NO_2 during the COVID-19 pandemic, we have further demonstrated how this methodology can be used for emergent research questions for which relying on observations or atmospheric models alone would be challenged by moderating influences, incomplete spatial coverage, and inaccuracies.

Several factors and limitations of our data and methods may contribute to the observed spread in the diesel share-ΔNO_2 relationship among cities. GEOS-CF's use of anthropogenic emissions from 2010 for all following years may under- or overestimate NO_2, especially in areas undergoing rapid changes in emissions. Our use of on-road transportation NO_x emissions as a proxy for NO_x from light-duty passenger vehicles (Figure 4) is an obvious simplification. This approach was necessary due to lack of globally consistent emissions inventories with information on NO_x from different types of on-road vehicles. There have been efforts to provide such information but only for specific regions or countries (e.g., Dallmann et al., 2013; Harkins et al., 2021; Osses et al., 2021). Additionally, our framework does not consider intracity differences in the type (i.e., gasoline versus diesel) of passenger vehicles that remained parked and off the road during the pandemic due to lack of data.

While our study incorporated changes in traffic into our machine learning approach, the pandemic impacted many forms of urban activity besides on-road traffic. NO_x emissions from the aviation, rail, and maritime sectors plummeted during COVID-19 (e.g., Rothengatter et al., 2021). We have not accounted for trends in these activities within XGBoost as we are challenged by a lack of city-specific time series data. Other exogenous events beyond the COVID-19 pandemic such as inclement weather could impact our calculation of ΔNO_2 but have also not been explicitly accounted for in our experimental design. However, recent studies point to on-road traffic, particularly passenger vehicles, as the primary driver of NO_2 reductions during the pandemic (Venter et al., 2020; Kerr et al., 2021). An analysis of ΔNO_2 against changes in traffic from the Apple Mobility Trends Reports in our 22 focus cities reveals a positive, albeit weak, relationship between ΔNO_2 and changes in traffic (Figure S8).

The number and distribution of *in-situ* monitors vary from city to city (Figure S1). Several focus cities have a large number of monitors that are relatively evenly distributed throughout the urban area, and we assume that the meta-site formed with these stations is broadly representative of overall urban NO_2. There are, however, other cities with substantially fewer monitors (e.g., Krakow, Poland; Figure S1) or spatially clustered monitors (e.g., Rotterdam, Netherlands; Figure S1). As was previously discussed for Berlin, monitors may lie in substantially different environments (e.g., traffic, suburban, urban background). If monitors are disproportionately sited in relatively non-polluted neighborhoods to monitor urban background pollution, we expect ΔNO_2 will be smaller than if monitors are disproportionately located in polluted neighborhoods or near sources of NO_2 beyond traffic.

Accounting for differences in traffic among cities and traffic's impact on NO_2 pollution requires spatially- and temporally resolved traffic data. Mobility datasets typically cover only specific regions or are cost prohibitive. Apple and Google have offered data on mobility trends during the pandemic, which is an important step to provide a globally consistent, open-access dataset on traffic trends. We found that Apple's Mobility Trends Reports offer greater granularity than Google's COVID-19 Community Mobility Reports for our focus cities; however, three of our 22 cities lack city-specific traffic trends, and we relied on country-level data (Table S1). Apple does not provide information about the representativeness of their mobility data against the overall population. It is possible that socioeconomic factors or cellphone preferences may lead to the Apple data being representative of a certain subset of the population in a given city. Political and

cultural differences across and within countries might also lead to different reactions and willingness to adhere to stay-at-home measures that may not be reflected in mobility data.

We obtained traffic counts directly from two of the focus cities (Berlin and Milan) who report their traffic data to C40 Cities and compared these counts with the Apple dataset. While these different datasets record intrinsically different quantities (number of passing vehicles at *in-situ* traffic counters versus anonymized mobile phone location data), these two datasets have demonstrably similar trends during the pandemic (Figure S9a-b). Recalculating bias-corrected ΔNO_2 with these *in-situ* traffic counts yields similar values as those calculated with the Apple dataset (Figure S9c-d). Neither the Apple dataset or *in-situ* counts for Milan and Berlin capture information on changes in vehicle speed. NO_x emissions generally increase with vehicle speed (Kean et al., 2003), and it is possible that changes in congestion and the types of roads driven on during the pandemic (e.g., local roads versus highways) impact average vehicle speeds and therefore NO_x emissions.

Despite similar diesel shares in Spanish, Croatian, and French focus cities, there is a spread of nearly ~30% in ΔNO_2 with Spanish and Croatian cities (Madrid, Barcelona, and Zagreb) experiencing larger ΔNO_2 than French cities (Figure 3). Passenger vehicles in Croatia and Spain are also 4.4 and 2.5 years older on average, respectively, than their French counterparts (European Automobile Manufacturers Association, 2021). Beyond these two countries, the proportion of vehicles belonging to different emission limit standards (i.e., Euro 1-6) may also vary across countries with the same or similar diesel shares and impact results. NO_x emission rates are not stable over diesel passenger vehicles' lifetimes and increase linearly with age (Chen and Borken-Kleefeld, 2016). The tendency for emission rates to increase with age may result in "effective diesel shares" that are larger than the ones used in our study, especially for focus cities with older passenger vehicle fleets. The role of vehicle age may explain some of the spread in Figure 3 and suggests that future policies to preferentially remove *older* diesel passenger vehicles from cities may have outsized impacted compared to removing newer diesel vehicles.

In spite of these limitations, our key findings are relevant for present-day and future policies. The temporary NO_2 reductions during the COVID-19 pandemic could be sustained through long-term policies to reduce the number of passenger vehicles in urban areas through, for example, policies such as congestion pricing or those that promote active transportation (e.g., cycling, walking). Should these policies be implemented, our results suggest that cities with larger diesel shares would experience larger NO_2 reductions. Beyond decreasing NO_2 and the associated public health damages, these types of policies would also slow climate change, decrease concentrations of other harmful pollutants such as particulate matter and O_3, and encourage healthier lifestyles if active forms of transportation replace passenger vehicles (e.g., Shindell et al., 2011). Focus cities such as Paris and Berlin are poised to ban most or all diesel passenger vehicles in the near future (C40 Cities Climate Leadership Group, 2019). We expect that our results will reinforce these efforts in Paris and Berlin and catalyze other cities to implement similar policies.

Acknowledgements
Funding for our study came from NASA through their Rapid Response and Novel Research in Earth Science (RRNES) initiative via grant #80NSSC20K1122. This work used The George Washington University's high-performance computing cluster, which is supported by

professional staff in The George Washington Information Technology and university-sponsored computation staff in the Milken Institute School of Public Health. We express our sincere appreciation to Shanju Xie, Cathy Bebelman, Amir Kayal, Lauren Simpson, and Elizabeth Parker (Auckland); Andreas Kerschbaumer and Martin Lutz (Berlin); William Bradley and Matthew Browning (London); Irene Burga, David Somers, Alexander Wikstrom, and Chet Edelman (Los Angeles); Álvaro Madrigal Montes de Oca, Fernanda Rivera, Stephanie Montero Bending, Daneila Muñoz, Monica Jaimes Palomera, Sergio Zirath Hernandez Villaseñor, and Patricia Camacho Rodriguez (Mexico City); Silvia Moroni, Manuela Ojan, Valentino Sevino, and Isabel Riboldi (Milan); Diego Jose Riveauz Marcet, Roberto Delagdo López, Juan Fernandez Bustamante, and Juan Fernandez Bustamante (Santiago) for collecting and sharing data with C40 Cities used for this study and for providing us insights. We also recognize Josh Miller, Joel Dreessen, Zifei Yang, Zifeng Lu, and Bryan Duncan for helpful discussions and the International Council on Clean Transit for providing data. NO_2 observations from the European air quality database, Airbase, are publicly available at www.ee a.europa.eu/data-and-maps/data/aqereporting-8. Apple Mobility Trends Reports and OxCGRT stay-at-home measure dates are available at covid19.apple.com/mobility and covidtracker.bsg.ox.ac.uk, respectively. NASA's GEOS-CF data are available at https://gmao.gsfc.nasa.gov/weather_prediction/GEOS-CF/. The emissions inventories used in this study can be found at jeodpp.jrc.ec.europa.eu/ftp/jrc-opendata/EDGAR/datasets/v50_AP/ (EDGAR), https://zenodo.org/record/3754964#.YQLwWC2ZPOQ (CEDS), and www.ceip.at/the-emep-grid/gridded-emissions (EMEP). The authors thank all those responsible for their support of these datasets.

References

Achakulwisut, P.; Brauer, M.; Hystad, P.; Anenberg, S. C. Global, National, and Urban Burdens of Paediatric Asthma Incidence Attributable to Ambient NO_2 Pollution: Estimates from Global Datasets. *Lancet Planet. Health* 2019, 3 (4), e166–e178. https://doi.org/10.1016/s2542-5196(19)30046-4.

Anenberg, S. C.; Miller, J.; Minjares, R.; Du, L.; Henze, D. K.; Lacey, F.; Malley, C. S.; Emberson, L.; Franco, V.; Klimont, Z.; Heyes, C. Impacts and Mitigation of Excess Diesel-Related NO_x Emissions in 11 Major Vehicle Markets. *Nature* 2017, 545 (7655), 467–471. https://doi.org/10.1038/nature22086.

Apple. COVID-19 Mobility Trends Reports. Apple, 2020. https://covid19.apple.com/mobility (accessed March 6, 2021).

Bey, I.; Jacob, D. J.; Yantosca, R. M.; Logan, J. A.; Field, B. D.; Fiore, A. M.; Li, Q.; Liu, H. Y.; Mickley, L. J.; Schultz, M. G. Global Modeling of Tropospheric Chemistry with Assimilated Meteorology: Model Description and Evaluation. *J. Geophys. Res.* 2001, 106 (D19), 23073–23095. https://doi.org/10.1029/2001jd000807.

C40 Cities Climate Leadership Group. *C40 Clean Air Cities Declaration: Planned actions to deliver commitments*; London, UK, 2019. https://www.c40knowledgehub.org/s/article/C40-

Clean-Air-Cities-Declaration-Planned-actions-to-deliver-commitments?language=en_US (accessed June 29, 2021).

Carslaw, D. C.; Murrells, T. P.; Andersson, J.; Keenan, M. Have Vehicle Emissions of Primary NO_2 Peaked? *Faraday Discuss.* 2016, 189, 439–454. https://doi.org/10.1039/c5fd00162e.

Chen, T.; Guestrin, C. XGBoost. In *Proceedings of the 22nd ACM SIGKDD International Conference on Knowledge Discovery and Data Mining*; ACM, 2016. https://doi.org/10.1145/2939672.2939785

Chen, Y.; Borken-Kleefeld, J. NO_x Emissions from Diesel Passenger Cars Worsen with Age. Environ. Sci. Technol. 2016, 50 (7), 3327–3332. https://doi.org/10.1021/acs.est.5b04704.

Cot, C.; Cacciapaglia, G.; Sannino, F. Mining Google and Apple Mobility Data: Temporal Anatomy for COVID-19 Social Distancing. *Sci. Rep.* 2021, 11 (1). https://doi.org/10.1038/s41598-021-83441-4.

Crippa, M.; Oreggioni, G.; Guizzardi, D.; Muntean, M.; Schaaf, E.; Lo Vullo, E.; Solazzo, E.; Monforti-Ferrario, F.; Olivier, J.G.J.; Vignati, E. *Fossil CO2 and GHG emissions of all world countries - 2019 Report*; EUR 29849 EN; Publications Office of the European Union: Luxembourg, 2019, ISBN 978-92-76-11100-9, doi:10.2760/687800, JRC117610.

Crippa, M.; Solazzo, E.; Huang, G.; Guizzardi, D.; Koffi, E.; Muntean, M.; Schieberle, C.; Friedrich, R.; Janssens-Maenhout, G. High Resolution Temporal Profiles in the Emissions Database for Global Atmospheric Research. *Sci. Data* 2020, 7 (1). https://doi.org/10.1038/s41597-020-0462-2.

Dallmann, T. R.; Kirchstetter, T. W.; DeMartini, S. J.; Harley, R. A. Quantifying On-Road Emissions from Gasoline-Powered Motor Vehicles: Accounting for the Presence of Medium- and Heavy-Duty Diesel Trucks. *Environ. Sci. Technol.* 2013, 47 (23), 13873–13881. https://doi.org/10.1021/es402875u.

Darmenov, A. S.; Da Silva, A. M. The Quick Fire Emissions Dataset (QFED): Documentation of versions 2.1, 2.2 and 2.4. *NASA Technical Report Series on Global Modeling and Data Assimilation* 38 (NASA/TM–2015–104606), 2015.

Degraeuwe, B.; Thunis, P.; Clappier, A.; Weiss, M.; Lefebvre, W.; Janssen, S.; Vranckx, S. Impact of Passenger Car NO_x Emissions on Urban NO_2 Pollution – Scenario Analysis for 8 European Cities. *Atmos. Environ.* 2017, 171, 330–337. https://doi.org/10.1016/j.atmosenv.2017.10.040.

Degraeuwe, B.; Pisoni, E.; Peduzzi, E.; De Meij, A.; Monforti-Ferrario, F.; Bodis, K.; Mascherpa, A.; Astorga-Llorens, M.; Thunis, P.; Vignati, E. *Urban NO_2 Atlas*; EUR 29943 EN; Publications Office of the European Union: Luxembourg, 2019, ISBN 978-92-76-10387-5, doi:10.2760/538816, JRC118193.

Diaz, S; Mock, P., Bernard, Y.; Bieker, G.; Pniewska, I.; Ragon, P.-L.; Rodriguez, F.; Tietge, U.; Wappelhorst, S. European vehicle market statistics 2020/21. International Council on Clean Transit, 2020. https://theicct.org/publications/european-vehicle-market-statistics-202021 (accessed April 14, 2021).

Ding, J.; A, R. J.; Eskes, H. J.; Mijling, B.; Stavrakou, T.; Geffen, J. H. G. M.; Veefkind, J. P. NO_x Emissions Reduction and Rebound in China Due to the COVID-19 Crisis. *Geophys. Res. Lett.* 2020, 47 (19). https://doi.org/10.1029/2020gl089912.

Dunlea, E. J.; Herndon, S. C.; Nelson, D. D.; Volkamer, R. M.; San Martini, F.; Sheehy, P. M.; Zahniser, M. S.; Shorter, J. H.; Wormhoudt, J. C.; Lamb, B. K.; Allwine, E. J.; Gaffney, J. S.; Marley, N. A.; Grutter, M.; Marquez, C.; Blanco, S.; Cardenas, B.; Retama, A.; Ramos Villegas, C. R.; Kolb, C. E.; Molina, L. T.; Molina, M. J. Evaluation of Nitrogen Dioxide Chemiluminescence Monitors in a Polluted Urban Environment. *Atmos. Chem. Phys.* 2007, 7 (10), 2691–2704. https://doi.org/10.5194/acp-7-2691-2007.

European Environment Agency. *Explaining Road Transport Emissions: A Non-technical Guide*; TH-04-16-016-EN-N; Publications Office of the European Union: Luxembourg, 2016. https://doi.org/10.2800/71804.

European Environment Agency. *Air Quality e-Reporting (AQ e-Reporting).* European Environment Agency, 2018. https://www.eea.europa.eu/data-and-maps/data/aqereporting-8 (accessed February 11, 2021).

European Automobile Manufacturers Association. *ACEA Report Vehicles in use Europe, January 2021*; European Automobile Manufacturers Association, 2021. https://www.acea.auto/publication/report-vehicles-in-use-europe-january-2021/ (accessed April 14, 2021).

Elguindi, N.; Granier, C.; Stavrakou, T.; Darras, S.; Bauwens, M.; Cao, H.; Chen, C.; Denier van der Gon, H. A. C.; Dubovik, O.; Fu, T. M.; Henze, D. K.; Jiang, Z.; Keita, S.; Kuenen, J. J. P.; Kurokawa, J.; Liousse, C.; Miyazaki, K.; Müller, J. -F.; Qu, Z.; Solmon, F.; Zheng, B. Intercomparison of Magnitudes and Trends in Anthropogenic Surface Emissions From Bottom-Up Inventories, Top-Down Estimates, and Emission Scenarios. *Earth's Future* 2020, 8 (8). https://doi.org/10.1029/2020ef001520.

Faustini, A.; Rapp, R.; Forastiere, F. Nitrogen Dioxide and Mortality: Review and Meta-Analysis of Long-Term Studies. *Eur. Respir. J.* 2014, 44 (3), 744–753. https://doi.org/10.1183/09031936.00114713.

Font, A.; Guiseppin, L.; Blangiardo, M.; Ghersi, V.; Fuller, G. W. A Tale of Two Cities: Is Air Pollution Improving in Paris and London? *Environ. Pollut.* 2019, 249, 1–12. https://doi.org/10.1016/j.envpol.2019.01.040.

Gkatzelis, G. I.; Gilman, J. B.; Brown, S. S.; Eskes, H.; Gomes, A. R.; Lange, A. C.; McDonald, B. C.; Peischl, J.; Petzold, A.; Thompson, C. R.; Kiendler-Scharr, A. The Global Impacts of

COVID-19 Lockdowns on Urban Air Pollution. *Elementa* 2021, 9 (1). https://doi.org/10.1525/elementa.2021.00176.

Geng, G.; Zhang, Q.; Martin, R. V.; Lin, J.; Huo, H.; Zheng, B.; Wang, S.; He, K. Impact of Spatial Proxies on the Representation of Bottom-up Emission Inventories: A Satellite-Based Analysis. *Atmos. Chem. Phys.* 2017, 17 (6), 4131–4145. https://doi.org/10.5194/acp-17-4131-2017.

Goldberg, D. L.; Anenberg, S. C.; Griffin, D.; McLinden, C. A.; Lu, Z.; Streets, D. G. Disentangling the Impact of the COVID-19 Lockdowns on Urban NO_2 From Natural Variability. *Geophys. Res. Lett.* 2020, 47 (17). https://doi.org/10.1029/2020gl089269.

Hale, T.; Angrist, N.; Goldszmidt, R.; Kira, B.; Petherick, A.; Phillips, T.; Webster, S.; Cameron-Blake, E.; Hallas, L.; Majumdar, S.; Tatlow, H. A Global Panel Database of Pandemic Policies (Oxford COVID-19 Government Response Tracker). *Nat. Hum. Behav.* 2021, 5 (4), 529–538. https://doi.org/10.1038/s41562-021-01079-8.

Harkins, C.; McDonald, B. C.; Henze, D. K.; Wiedinmyer, C. A Fuel-Based Method for Updating Mobile Source Emissions during the COVID-19 Pandemic. *Environ. Res. Lett.* 2021, 16 (6), 065018. https://doi.org/10.1088/1748-9326/ac0660.

Hoesly, R. M.; Smith, S. J.; Feng, L.; Klimont, Z.; Janssens-Maenhout, G.; Pitkanen, T.; Seibert, J. J.; Vu, L.; Andres, R. J.; Bolt, R. M.; Bond, T. C.; Dawidowski, L.; Kholod, N.; Kurokawa, J.; Li, M.; Liu, L.; Lu, Z.; Moura, M. C. P.; O'Rourke, P. R.; Zhang, Q. Historical (1750–2014) Anthropogenic Emissions of Reactive Gases and Aerosols from the Community Emissions Data System (CEDS). *Geosci. Model Dev.* 2018, 11 (1), 369–408. https://doi.org/10.5194/gmd-11-369-2018.

Hu, L.; Keller, C. A.; Long, M. S.; Sherwen, T.; Auer, B.; Da Silva, A.; Nielsen, J. E.; Pawson, S.; Thompson, M. A.; Trayanov, A. L.; Travis, K. R.; Grange, S. K.; Evans, M. J.; Jacob, D. J. Global Simulation of Tropospheric Chemistry at 12.5 Km Resolution: Performance and Evaluation of the GEOS-Chem Chemical Module (V10-1) within the NASA GEOS Earth System Model (GEOS-5 ESM). *Geosci. Model Dev.* 2018, 11 (11), 4603–4620. https://doi.org/10.5194/gmd-11-4603-2018.

Ivatt, P. D.; Evans, M. J. Improving the Prediction of an Atmospheric Chemistry Transport Model Using Gradient-Boosted Regression Trees. *Atmos. Chem. Phys.* 2020, 20 (13), 8063–8082. https://doi.org/10.5194/acp-20-8063-2020.

Janssens-Maenhout, G.; Crippa, M.; Guizzardi, D.; Dentener, F.; Muntean, M.; Pouliot, G.; Keating, T.; Zhang, Q.; Kurokawa, J.; Wankmüller, R.; Denier van der Gon, H.; Kuenen, J. J. P.; Klimont, Z.; Frost, G.; Darras, S.; Koffi, B.; Li, M. HTAP_v2.2: A Mosaic of Regional and Global Emission Grid Maps for 2008 and 2010 to Study Hemispheric Transport of Air Pollution. *Atmos. Chem. Phys.* 2015, 15 (19), 11411–11432. https://doi.org/10.5194/acp-15-11411-2015.

Jonson, J. E.; Borken-Kleefeld, J.; Simpson, D.; Nyíri, A.; Posch, M.; Heyes, C. Impact of Excess NO_x Emissions from Diesel Cars on Air Quality, Public Health and Eutrophication in Europe. *Environ. Res. Lett.* 2017, 12 (9), 094017. https://doi.org/10.1088/1748-9326/aa8850.

Kean, A. J.; Harley, R. A.; Kendall, G. R. Effects of Vehicle Speed and Engine Load on Motor Vehicle Emissions. *Environ. Sci. Technol.* 2003, 37 (17), 3739–3746. https://doi.org/10.1021/es0263588.

Kerr, G. H.; Goldberg, D. L.; Anenberg, S. C. COVID-19 Pandemic Reveals Persistent Disparities in Nitrogen Dioxide Pollution. *Proc. Natl. Acad. Sci. USA* 2021, 118 (30), e2022409118. https://doi.org/10.1073/pnas.2022409118.

Keller, C. A.; Long, M. S.; Yantosca, R. M.; Da Silva, A. M.; Pawson, S.; Jacob, D. J. HEMCO v1.0: A Versatile, ESMF-Compliant Component for Calculating Emissions in Atmospheric Models. *Geosci. Model Dev.*, 2014, 7, 1409–1417. https://doi.org/10.5194/gmd-7-1409-2014.

Keller, C. A.; Evans, M. J.; Knowland, K. E.; Hasenkopf, C. A.; Modekurty, S.; Lucchesi, R. A.; Oda, T.; Franca, B. B.; Mandarino, F. C.; Díaz Suárez, M. V.; Ryan, R. G.; Fakes, L. H.; Pawson, S. Global Impact of COVID-19 Restrictions on the Surface Concentrations of Nitrogen Dioxide and Ozone. *Atmos. Chem. Phys.* 2021a, 21 (5), 3555–3592. https://doi.org/10.5194/acp-21-3555-2021.

Keller, C. A.; Knowland, K. E.; Duncan, B. N.; Liu, J.; Anderson, D. C.; Das, S.; Lucchesi, R. A.; Lundgren, E. W.; Nicely, J. M.; Nielsen, E.; Ott, L. E.; Saunders, E.; Strode, S. A.; Wales, P. A.; Jacob, D. J.; Pawson, S. Description of the NASA GEOS Composition Forecast Modeling System GEOS-CF v1.0. *J. Adv. Model. Earth Syst.* 2021b, 13(4). https://doi.org/10.1029/2020ms002413.

Khomenko, S.; Cirach, M.; Pereira-Barboza, E.; Mueller, N.; Barrera-Gómez, J.; Rojas-Rueda, D.; de Hoogh, K.; Hoek, G.; Nieuwenhuijsen, M. Premature Mortality Due to Air Pollution in European Cities: A Health Impact Assessment. *Lancet Planet. Health* 2021, 5 (3), e121–e134. https://doi.org/10.1016/s2542-5196(20)30272-2.

Kiesewetter, G.; Borken-Kleefeld, J.; Schöpp, W.; Heyes, C.; Thunis, P.; Bessagnet, B.; Terrenoire, E.; Gsella, A.; Amann, M. Modelling NO_2 Concentrations at the Street Level in the GAINS Integrated Assessment Model: Projections under Current Legislation. *Atmos. Chem. Phys.* 2014, 14 (2), 813–829. https://doi.org/10.5194/acp-14-813-2014.

Knowland, K. E.; Keller, C. A.; Lucchesi R.A. 2020. File Specification for GEOS-CF Products. *GMAO Office Note No. 17 (Version 1.1), 37 pp, available from http://gmao.gsfc.nasa.gov/pubs/office_notes*, 2020.

Kroll, J. H.; Heald, C. L.; Cappa, C. D.; Farmer, D. K.; Fry, J. L.; Murphy, J. G.; Steiner, A. L. The Complex Chemical Effects of COVID-19 Shutdowns on Air Quality. *Nat. Chem.* 2020, 12 (9), 777–779. https://doi.org/10.1038/s41557-020-0535-z.

Lamsal, L. N.; Martin, R. V.; van Donkelaar, A.; Steinbacher, M.; Celarier, E. A.; Bucsela, E.; Dunlea, E. J.; Pinto, J. P. Ground-Level Nitrogen Dioxide Concentrations Inferred from the Satellite-Borne Ozone Monitoring Instrument. *J. Geophys. Res.* 2008, 113 (D16). https://doi.org/10.1029/2007jd009235.

Liu, J.; Lipsitt, J.; Jerrett, M.; Zhu, Y. Decreases in Near-Road NO and NO_2 Concentrations during the COVID-19 Pandemic in California. *Environ. Sci. Technol. Lett.* 2020, 8 (2), 161–167. https://doi.org/10.1021/acs.estlett.0c00815.

Long, M. S.; Yantosca, R.; Nielsen, J. E.; Keller, C. A.; da Silva, A.; Sulprizio, M. P.; Pawson, S.; Jacob, D. J. Development of a Grid-Independent GEOS-Chem Chemical Transport Model (v9-02) as an Atmospheric Chemistry Module for Earth System Models. *Geosci. Model Dev*, 2015, 8, 595–602. https://doi.org/10.5194/gmd-8-595-2015.

Lundberg, S.; Lee, S.-I. An unexpected unity among methods for interpreting model predictions. *arXiv*, 2016. arXiv:1611.07478.

Lundberg, S.; Lee, S.-I. A Unified Approach to Interpreting Model Predictions. In *31st Conference on Neural Information Processing Systems (NIPS 2017),* Long Beach, CA, 2016. arXiv:1705.07874.

Mareckova, K.; Pinterits, M; Ullrich, B.; Wankmueller, R.; Mandl N. Review of emission data reported under the LRTAP Convention and NEC Directive. EMEP Centre on Emission Inventories and Projections, 2(2017), p. 52, 10.1029/2009JD011823

McDonald, B. C.; McBride, Z. C.; Martin, E. W.; Harley, R. A. High-Resolution Mapping of Motor Vehicle Carbon Dioxide Emissions. *J. Geophys. Res. Atmos.* 2014, 119 (9), 5283–5298. https://doi.org/10.1002/2013jd021219.

McDuffie, E. E.; Smith, S. J.; O'Rourke, P.; Tibrewal, K.; Venkataraman, C.; Marais, E. A.; Zheng, B.; Crippa, M.; Brauer, M.; Martin, R. V. A Global Anthropogenic Emission Inventory of Atmospheric Pollutants from Sector- and Fuel-Specific Sources (1970–2017): An Application of the Community Emissions Data System (CEDS). *Earth Syst. Sci. Data* 2020, 12 (4), 3413–3442. https://doi.org/10.5194/essd-12-3413-2020.

Osses, M.; Rojas, N.; Ibarra, C.; Valdebenito, V.; Laengle, I.; Pantoja, N.; Osses, D.; Basoa, K.; Tolvett, S.; Huneeus, N.; Gallardo, L.; Gómez, B. High-Definition Spatial Distribution Maps of on-Road Transport Exhaust Emissions in Chile, 1990–2020, 2021. *Earth Syst. Sci. Data Discuss.* https://doi.org/10.5194/essd-2021-218.

Rothengatter, W.; Zhang, J.; Hayashi, Y.; Nosach, A.; Wang, K.; Oum, T. H. Pandemic Waves and the Time after Covid-19 – Consequences for the Transport Sector. *Transport Policy* 2021, 110, 225–237. https://doi.org/10.1016/j.tranpol.2021.06.003.

Shapley, L. S. 17. A Value for n-Person Games. In Contributions to the Theory of Games (AM-28), Volume II; Princeton University Press, 1953; pp 307–318. https://doi.org/10.1515/9781400881970-018.

Shindell, D.; Faluvegi, G.; Walsh, M.; Anenberg, S. C.; Van Dingenen, R.; Muller, N. Z.; Austin, J.; Koch, D.; Milly, G. Climate, Health, Agricultural and Economic Impacts of Tighter Vehicle-Emission Standards. *Nature Clim Change* 2011, 1 (1), 59–66. https://doi.org/10.1038/nclimate1066.

Tietge, U.; Díaz, S. *Cities driving diesel out of the European car market*. International Council on Clean Transit, 2017. https://theicct.org/blogs/staff/cities-driving-diesel-out-european-car-market (accessed July 22, 2021).

Vadrevu, K. P.; Eaturu, A.; Biswas, S.; Lasko, K.; Sahu, S.; Garg, J. K.; Justice, C. Spatial and Temporal Variations of Air Pollution over 41 Cities of India during the COVID-19 Lockdown Period. *Sci. Rep.* 2020, 10 (1). https://doi.org/10.1038/s41598-020-72271-5.

Venter, Z. S.; Aunan, K.; Chowdhury, S.; Lelieveld, J. COVID-19 Lockdowns Cause Global Air Pollution Declines. *Proc. Natl. Acad. Sci. USA* 2020, 117 (32), 18984–18990. https://doi.org/10.1073/pnas.2006853117.

von Schneidemesser, E.; Kuik, F.; Mar, K. A.; Butler, T. Potential Reductions in Ambient NO 2 Concentrations from Meeting Diesel Vehicle Emissions Standards. *Environ. Res. Lett.* 2017, 12 (11), 114025. https://doi.org/10.1088/1748-9326/aa8c84.

von Schneidemesser, E.; Sibiya, B.; Caseiro, A.; Butler, T.; Lawrence, M. G.; Leitao, J.; Lupascu, A.; Salvador, P. Learning from the COVID-19 Lockdown in Berlin: Observations and Modelling to Support Understanding Policies to Reduce NO_2. Atmospheric Environment: X 2021, 12, 100122. https://doi.org/10.1016/j.aeaoa.2021.100122.

Weiss, M.; Bonnel, P.; Hummel, R.; Provenza, A.; Manfredi, U. On-Road Emissions of Light-Duty Vehicles in Europe. *Environ. Sci. Technol.* 2011, 45 (19), 8575–8581. https://doi.org/10.1021/es2008424.

Supporting Information

Text S1. Inclusion of non-European Union cities

We obtain *in-situ* measurements and diesel shares from four additional cities outside Europe (Auckland, Mexico City, Los Angeles, and Santiago) that report data to C40 Cities. These cities generally have lower diesel shares than European cities (Table S1) and specifically allow us to test whether our results are robust for cities with these large diesel shares. Using the additional global datasets (e.g., GEOS-CF, Apple Mobility Trends Reports) and methods described in the main text, we calculated bias-corrected NO_2 and ΔNO_2 for these four additional cities.

The inclusion of these four cities supports our main conclusions, mainly that these cities with smaller diesel shares generally experienced smaller decreases in NO_2 during the pandemic (Figures S6-S7). These results also speak to our broader methodological framework, indicating that future studies can leverage these methods and incorporate *in-situ* NO_2 observations, traffic data, and diesel shares from any urban area to understand the impact of diesel passenger vehicles on urban NO_2 pollution.

Table S1. Focus cities and information about their vehicle fleets, traffic data, and in-situ monitor networks. *Unless otherwise indicated, in-situ monitors are taken from the European air quality database, AirBase, maintained by the European Environment Agency. Rows in grey denote cities outside of the European Union included in the sensitivity analysis.*

City	Share of passenger diesel vehicles [%]	Number of *in-situ* monitors	Traffic
Athens, Greece	8.1[a]	4	city-level
Barcelona, Spain	58.7[a]	7	city-level
Berlin, Germany	31.7[a]	17	city-level
Budapest, Hungary	31.5[a]	5	city-level
Copenhagen, Denmark	30.9[a]	3	city-level
Helsinki, Finland	27.9[a]	3	city-level
Krakow, Poland	31.6[a]	3	city-level
London, United Kingdom	39.0[a]	126	city-level
Madrid, Spain	58.7[a]	24	city-level
Marseille, France	58.9[a]	3	city-level
Milan, Italy	44.2[a]	5	city-level
Munich, Germany	31.7[a]	4	city-level

Paris, France	58.9[a]	10	city-level
Prague, Czechia	35.9[a]	9	city-level
Rome, Italy	44.2[a]	13	city-level
Rotterdam, Netherlands	14.0[a]	8	city-level
Sofia, Bulgaria	43.1[c]	5	country-level
Stockholm, Sweden	35.5[a]	4	city-level
Vienna, Austria	55.0[a]	15	city-level
Vilnius, Lithuania	69.2[a]	4	country-level
Warsaw, Poland	31.6[a]	3	city-level
Zagreb, Croatia	52.4[a]	2	country-level
Auckland, New Zealand	8.3[b]	7[b]	city-level
Los Angeles, United States	0.4[b]	15[b]	city-level[d]
Mexico City, Mexico	0.2[b]	32[b]	city-level
Santiago, Chile	7.1[b]	9[b]	city-level

[a] Data derived from European Automobile Manufacturers Association.
[b] Based on data reported by city agencies to C40 Cities.
[c] Data derived from ICCT.
[d] City-level traffic data for Los Angeles represent an average over Los Angeles and Orange counties.

Table S2. *Input variables used in the machine learning algorithm, XGBoost. All variables from GEOS-CF represent near-surface values (lowest model level; > 985 hPa).*

Family and variables	Source
Meteorology: eastward wind, northward wind, fractional cloud cover, surface pressure, total precipitation, air temperature, planetary boundary layer height, specific humidity, relative humidity, sea level pressure	GEOS-CF
Composition: CO, NO_2, O_3, $PM_{2.5}$, SO_2	GEOS-CF
Mobility: Traffic	Apple mobility trends report

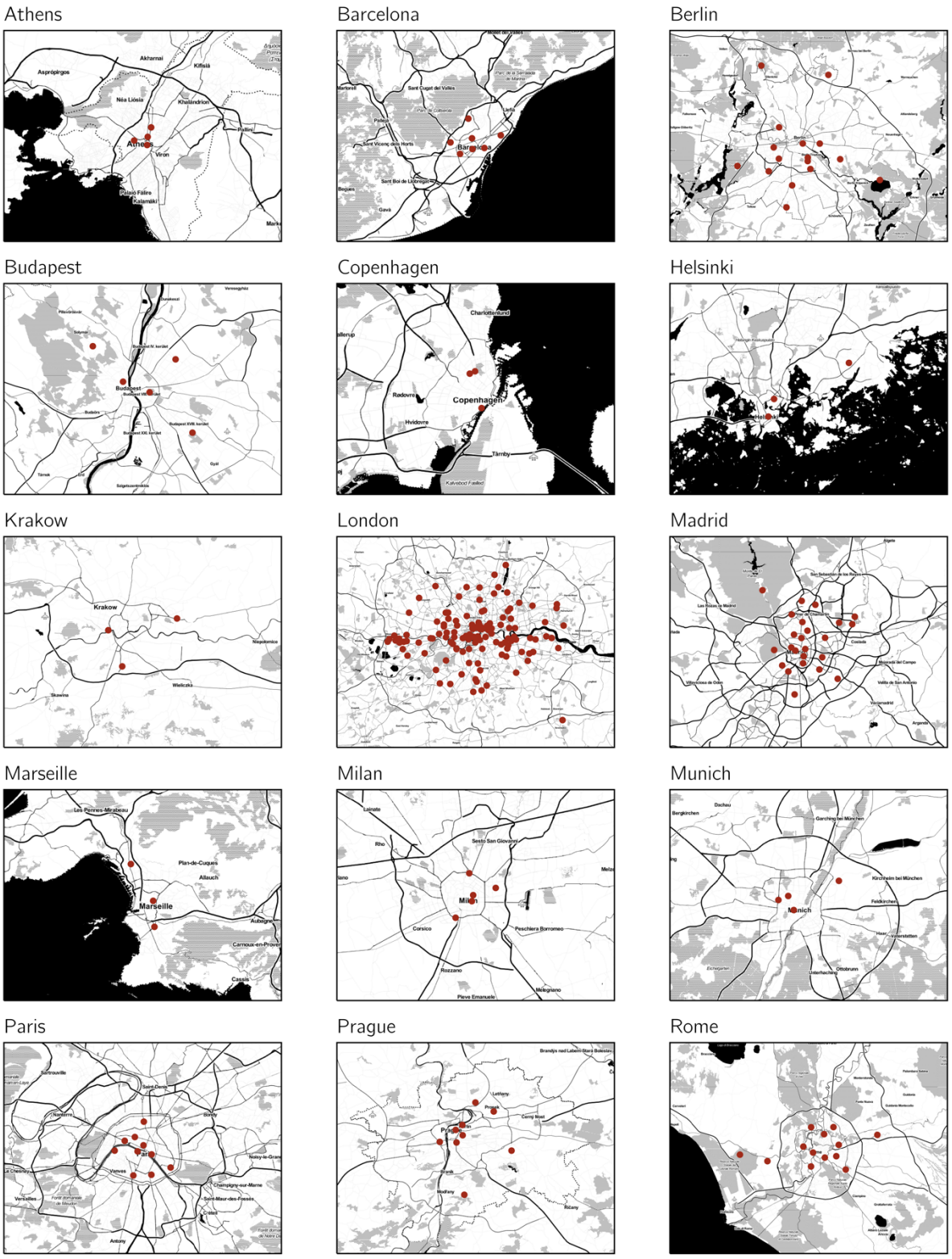

Figure S1. Location of in-situ NO_2 monitors in focus cities. *Bodies of water are denoted in black, and grey stippling indicates city parks or other green spaces.*

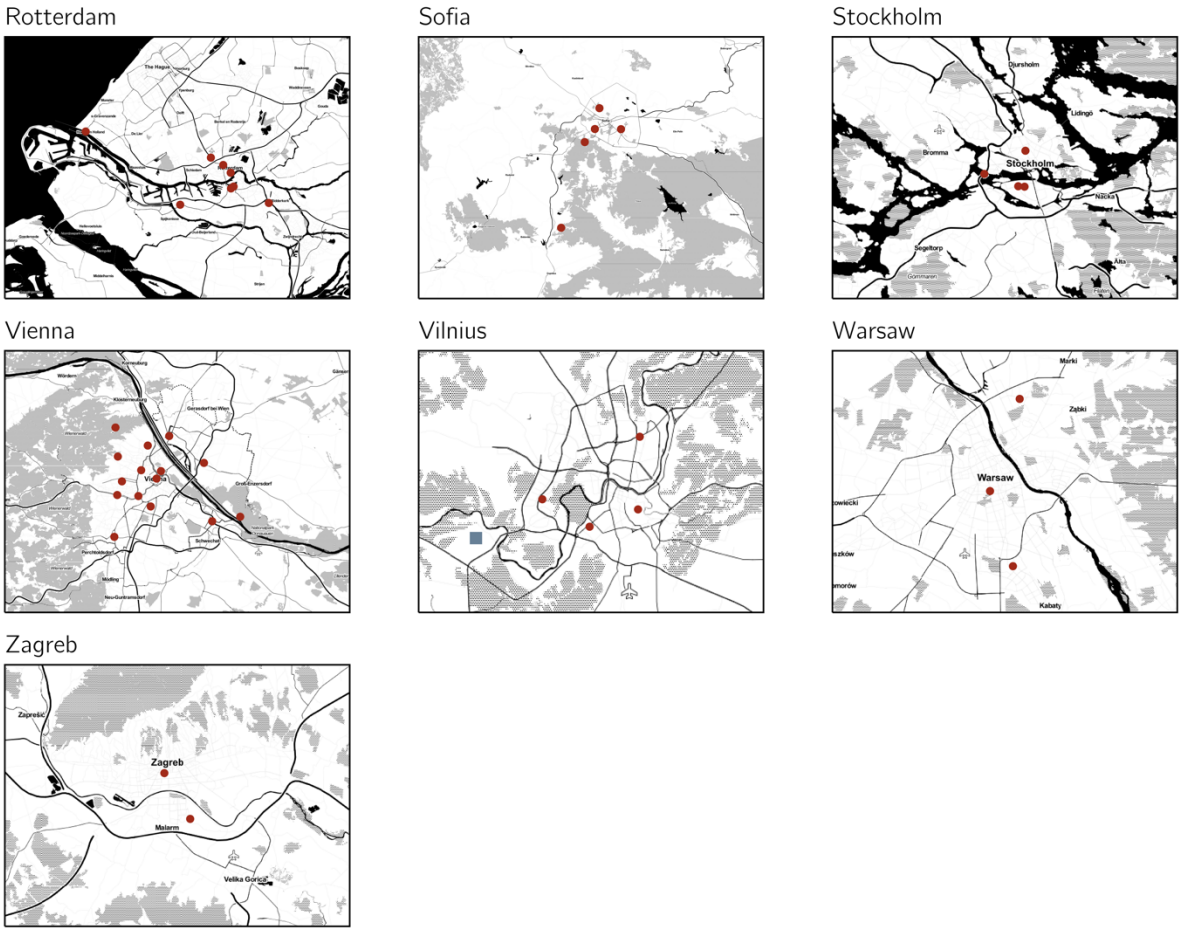

Figure S1 (continued). *The blue square in the map of Vilnius indicates the location of the natural gas- and mazut-burning Vilnius Heat Plant.*

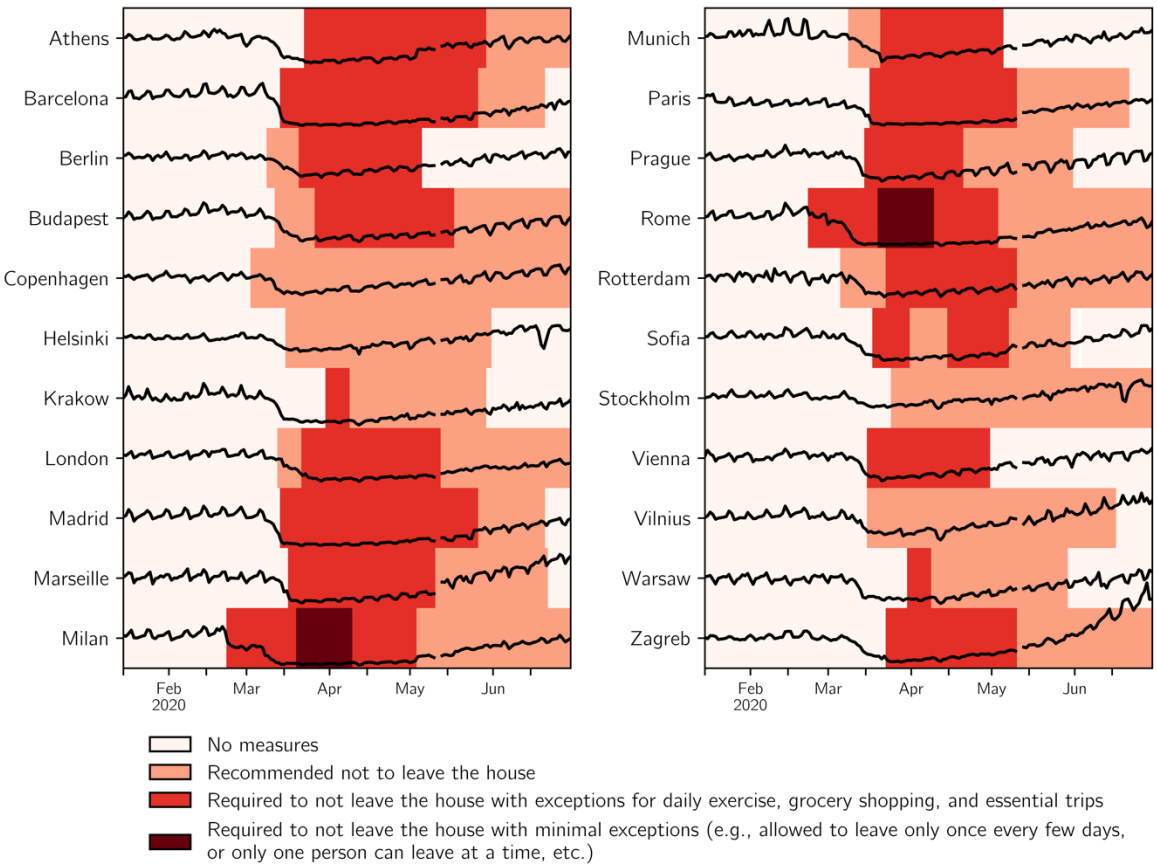

Figure S2. Focus cities' traffic patterns and stay-at-home measures. *Black time series qualitatively show city- or county-specific traffic volumes from the Apple Mobility Trends Reports relative to a baseline volume on 13 January 2020. Data for 11-12 May 2020 are not available. Colors indicate national-level stay-at-home recommendations or requirements for the country containing focus cities. Note that the different stay-at-home categories may not apply to every region within a country.*

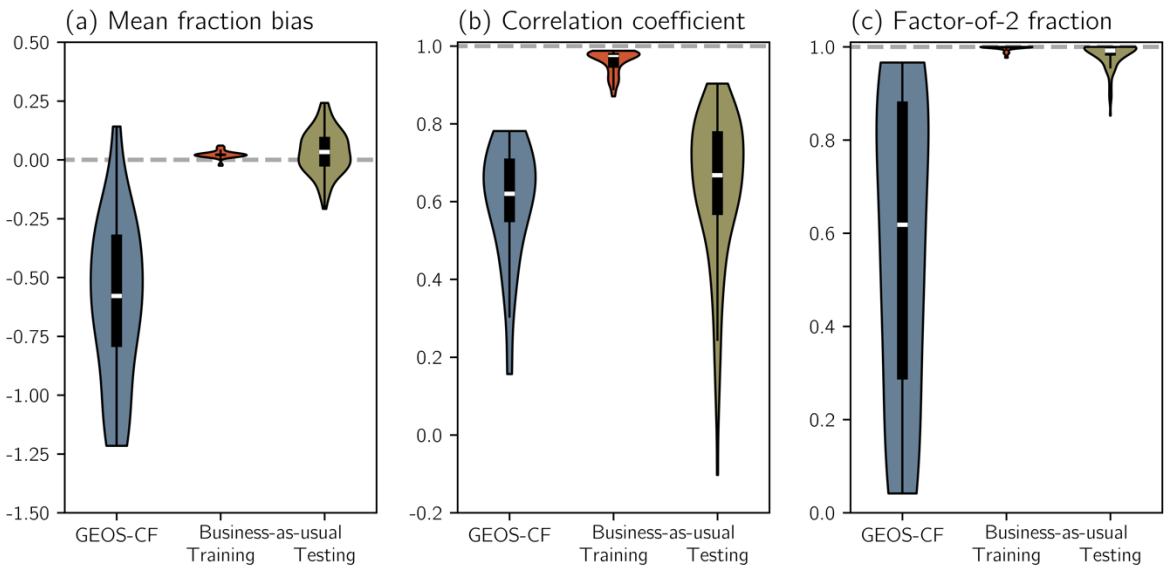

Figure S3. Evaluation metrics measuring the performance of NO_2 from GEOS-CF and the training and testing sets of the bias-corrected business-as-usual NO_2 against observed NO_2 for 2019. *Violins for GEOS-CF correspond to metrics for each focus city, while violins for the training and testing sets correspond to metrics from individual folds of the k-fold cross validation for each city. The median values, first and third quartiles, and extrema are denoted by the white lines, boxes, and whiskers, respectively, if space within violins allows. Dashed grey lines indicate the value of each metric for a model that perfectly matches the observed data.*

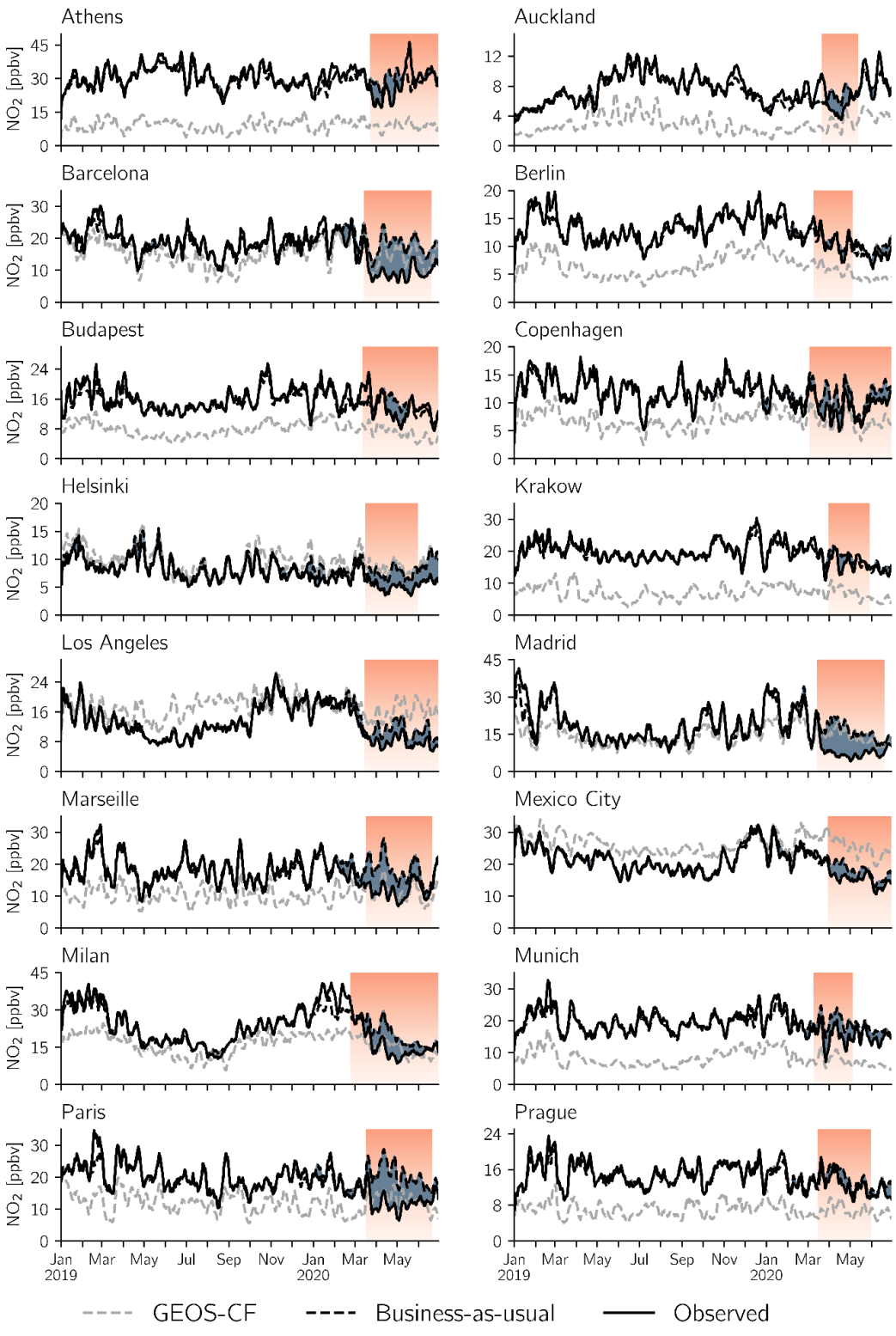

Figure S4. *Same as Figure 2a in the main text but for other focus cities.*

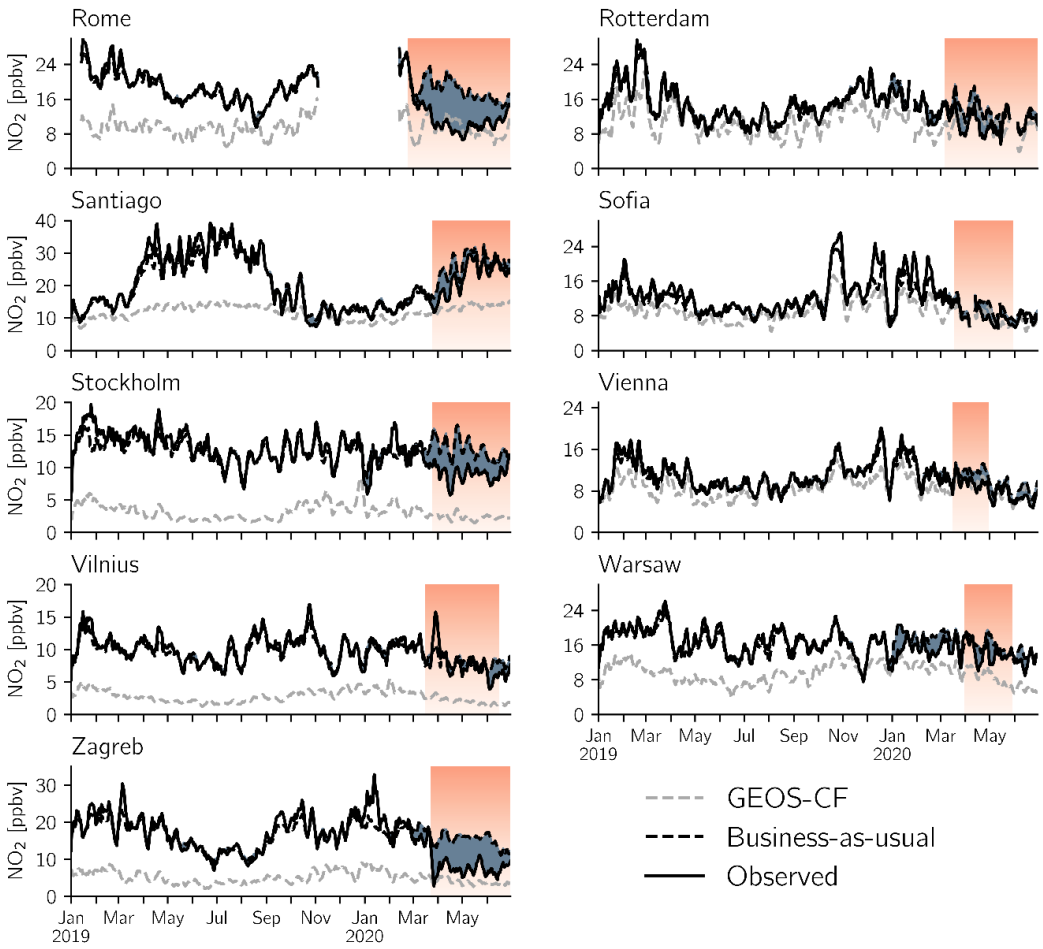

Figure S4 (continued).

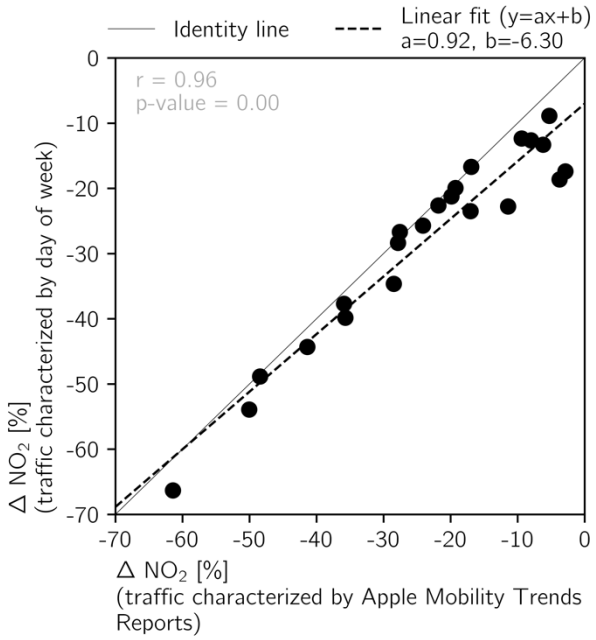

Figure S5. Comparison of ΔNO_2 determined by replacing daily traffic volume with integers corresponding to the day of the week versus ΔNO_2 determined with Apple Mobility Trends Reports. *Each point corresponds to a different focus city. The plot's legend indicates the form and coefficients of the linear regression used to describe the relationship between ΔNO_2 from the two different data sources, and inset text shows the correlation coefficient and p-value.*

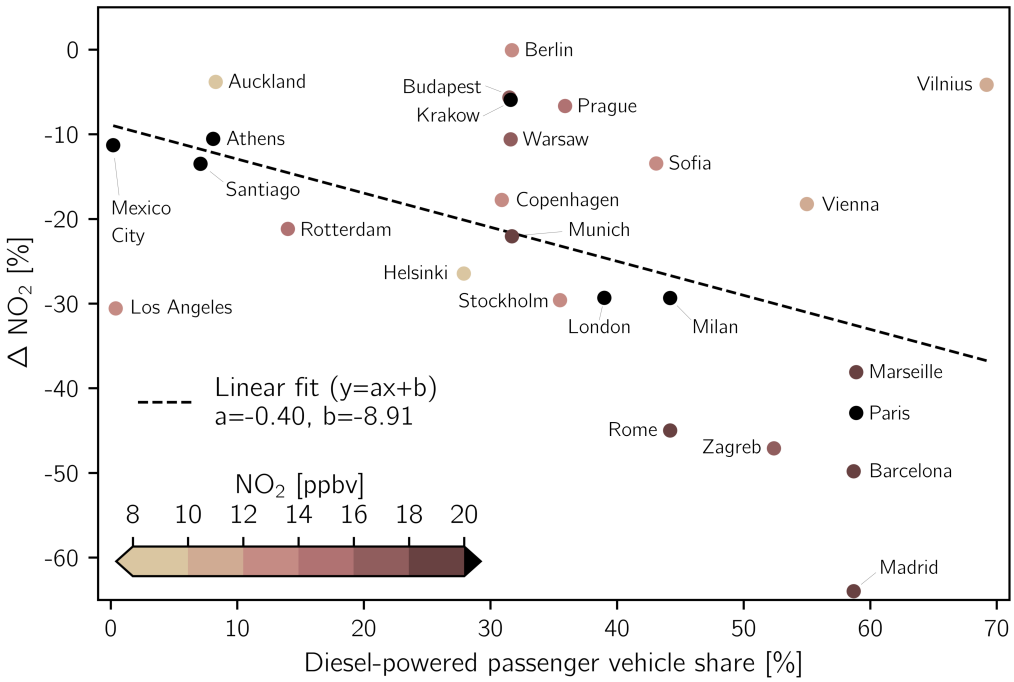

Figure S6. *Same as Figure 3 in the main text but ΔNO_2 is calculated over 15 March 2020 - 15 June 2020 for all cities rather than using the dates of country-specific stay-at-home measures (r = -0.47, p = 0.02).*

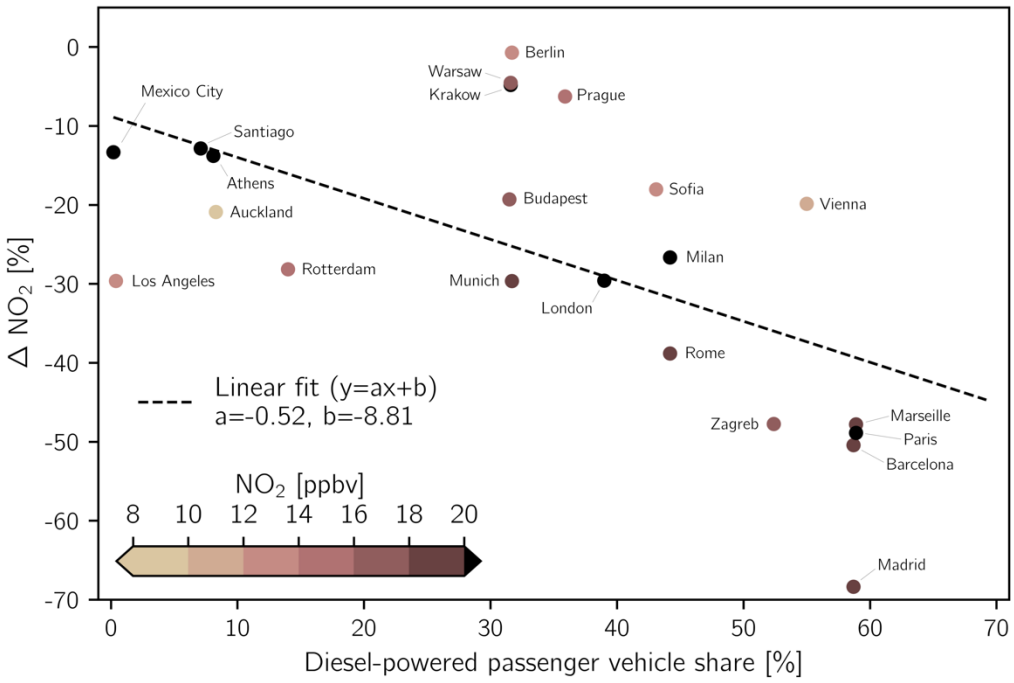

Figure S7. *Same as Figure 3 in the main text but ΔNO_2 is calculated only for days with required stay-at-home measures, denoted by the red and maroon colors in Figure S2 (r = -0.58; p < 0.01). Copenhagen, Helsinki, Stockholm, and Vilnius did not have required measures (Figure S2) and are thus not included in this figure.*

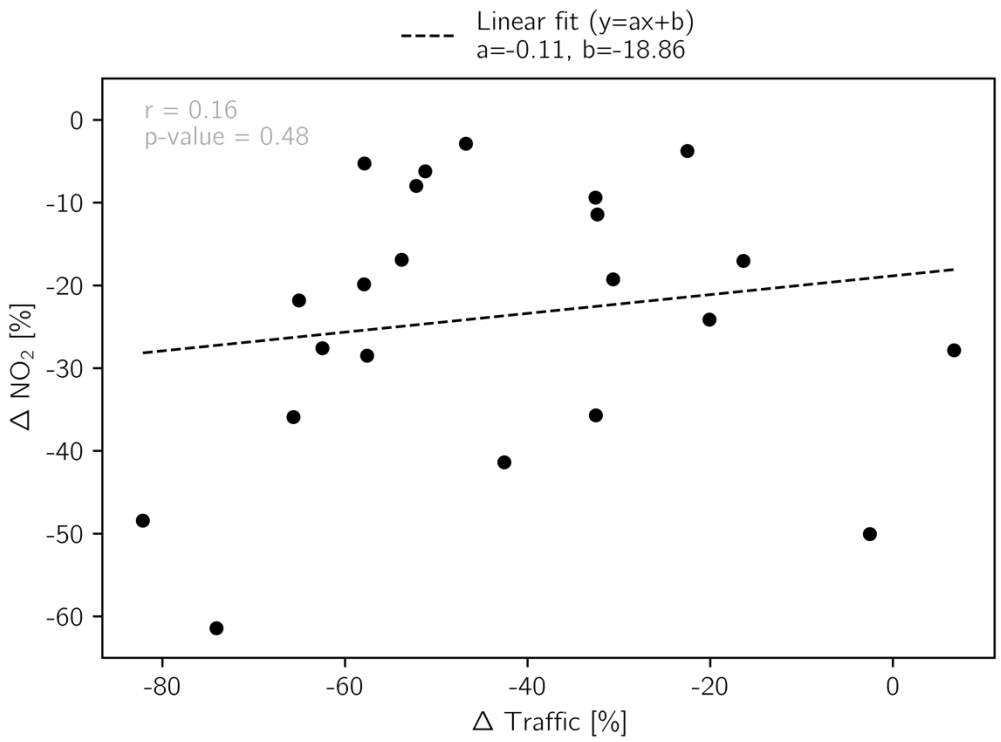

Figure S8. Association of change in traffic with ΔNO_2 for focus cities. *Both ΔNO_2 and ΔTraffic are averaged over days with country-specific recommended or required stay-at-home measures. Each point corresponds to a different focus city. The plot's legend indicates the form and coefficients of the linear regression used to describe the relationship between ΔNO_2 and ΔTraffic, and inset text shows the correlation coefficient and p-value.*

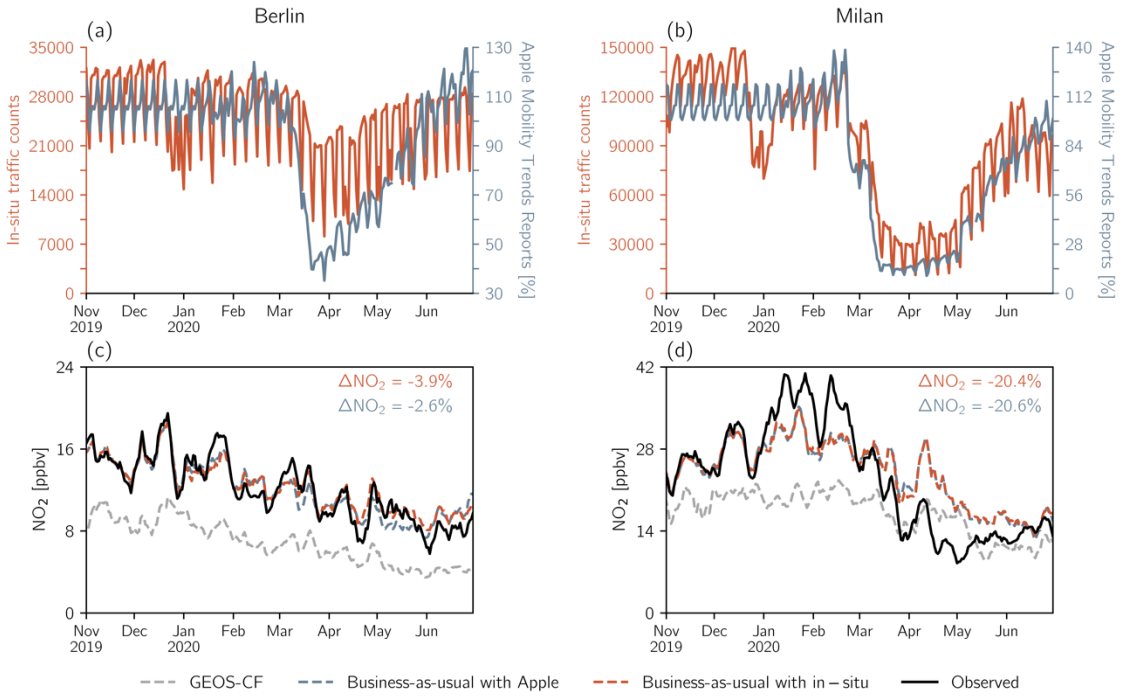

Figure S9. Comparison of traffic trends and business-as-usual NO_2 in Berlin and Milan using different traffic datasets. *(a)-(b) Traffic trends from in-situ traffic counters and Apple Mobility Trends Reports. (c)-(d) GEOS-CF, observed, and business-as-usual NO_2 concentrations calculated with the different traffic datasets. Text in the upper right corners of (c)-(d) indicates ΔNO_2 determined using the two different input traffic datasets.*